Comput. Methods Appl. Mech. Engrg. 268 (2014) 451–474

Contents lists available at ScienceDirect

Comput. Methods Appl. Mech. Engrg.

journal homepage: www.elsevier.com/locate/cma

Geometrically exact beam finite element formulated on the special Euclidean group $SE(3)$

V. Sonneville [a,*], A. Cardona [b], O. Brüls [a]

[a] Department of Aerospace and Mechanical Engineering (LTAS), University of Liège, Chemin des Chevreuils, 1 (B52), 4000 Liège, Belgium
[b] Universidad Nacional Litoral - Conicet, CIMEC-INTEC, Güemes 3450, 3000 Santa Fe, Argentina

ARTICLE INFO

Article history:
Received 16 April 2013
Received in revised form 3 October 2013
Accepted 8 October 2013
Available online 23 October 2013

Keywords:
Dynamic beam
Finite element
Lie group
Special Euclidean group

ABSTRACT

This paper describes a dynamic formulation of a straight beam finite element in the setting of the special Euclidean group $SE(3)$. First, the static and dynamic equilibrium equations are derived in this framework from variational principles. Then, a non-linear interpolation formula using the exponential map is introduced. It is shown that this framework leads to a natural coupling in the interpolation of the position and rotation variables. Next, the discretized internal and inertia forces are developed. The semi-discrete equations of motion take the form of a second-order ordinary differential equation on a Lie group, which is solved using a Lie group time integration scheme. It is remarkable that no parameterization of the nodal variables needs to be introduced and that the proposed Lie group framework leads to a compact and easy-to-implement formulation. Some important numerical and theoretical aspects leading to a computationally efficient strategy are highlighted and discussed. For instance, the formulation leads to invariant tangent stiffness and mass matrices under rigid body motions and a locking free element. The proposed formulation is successfully tested in several numerical static and dynamic examples.

1. Introduction

Modelling techniques in structural mechanics are usually based on position variables with respect to an inertial frame and their derivatives. For instance the potential energy in a gravitational field depends on the position, the kinetic energy depends on the time derivative of the position, that is the velocity, and the strain energy depends on the spatial derivatives of the position, namely the deformation gradient. The description of rigid bodies, beams or shells rely on kinematic assumptions on the position of their material points [1–4]. This can be made either by introducing rotation variables which account for some orientations [1,2] or without introducing any rotation field [5]. A comparison of the two approaches is available in [6]. The first approach, with rotation variables, is considered here. The development of the equations of mechanics under the kinematic assumptions leads in general to coupled equilibrium equations that govern both the rotation and the position variables. The rotations belong to a non-linear space, $SO(3)$, so that their general treatment is not trivial. Several methods have been explored to represent rotation variables such as the parametrization of rotation [1], the director vector method [7] or the Lie group methods [3,8–10]. In this paper, a Lie group method is studied, which is based on the differential geometry of the non-linear configuration space. The Lie group $\mathbb{R}^3 \times SO(3)$, which assumes that the compositions of the translations and the rotations are uncoupled, has been widely used for rigid body or beam formulations [1–3,11,12]. This choice of uncoupled composition rule implies that the finite element interpolation of the rotation and translation field of a beam are uncoupled.

* Corresponding author. Tel.: +32 43669513.
E-mail addresses: v.sonneville@ulg.ac.be (V. Sonneville), acardona@intec.unl.edu.ar (A. Cardona), o.bruls@ulg.ac.be (O. Brüls).

0045-7825/$ - see front matter © 2013 Elsevier B.V. All rights reserved.
http://dx.doi.org/10.1016/j.cma.2013.10.008

In contrast, the helicoidal approximation proposed in [13] and the strain-based approach in [14] lead to a coupled representation of the translation and rotation fields. Here, we consider the Lie group $SE(3) = \mathbb{R}^3 \rtimes SO(3)$, called the special Euclidean group, for which the compositions of translations and rotations are inherently coupled. The so-called screw-theory consists essentially in the study of this group and its algebra, and has been applied by several researchers in robotics and mechanism theory [15–18].

In this paper, a straight beam finite element formulation is developed. First, the continuous equilibrium equations in the $SE(3)$ framework are derived from a variational principle. Then, a spatial discretization of the beam is introduced by a nonlinear interpolation method of nodal values and the discrete problem is formulated. The representation of the rotations by interpolation of the nodal rotation variables is a non-trivial issue due to the non-linearity of the configuration space. For example, [3,11] defined an interpolation method based on the increments of the rotations and [12] proposed to interpolate the relative rotation matrix. In these references, the positions and the rotations are interpolated separately since they are considered to be fundamentally independent. In contrast, the $SE(3)$ Lie group framework used in this paper introduces a natural coupling of the position and the rotation variables thanks to an exponential interpolation method and exhibits important theoretical and numerical advantages. The equations of motion of the discrete mechanical system take the form of second-order ordinary differential equations on the Lie group. The equations are then solved using the generalized-α Lie group time integration scheme proposed in [8,10], which is closely related to the Lie group integrators developed in [19–21]. Let us mention that interpolation methods in the $SE(3)$ framework have been addressed in [22,23] for motion interpolation of rigid bodies. Using the $SE(3)$ framework, [24] proposed a method for beam finite element based on the manifold structure, that is using the same composition rule as the group $\mathbb{R}^3 \times SO(3)$, and [25] developed a linear beam formulation according to the screw theory.

The proposed approach relies on a rigorous mathematical framework based on the Lie group theory. Since a Lie group solver is used, it is remarkable that the equilibrium equation is formulated in a parameterization-free way and that no parameterization of the nodal variables needs to be introduced. The theory naturally leads to a frame-invariant, compact and elegant formulation of the beam finite element. Thanks to the simplicity of the formulation, the internal forces and the tangent stiffness matrix can be integrated exactly over the length of the element. Difficulties related to the parameterization of rotations or to locking problems are also automatically avoided.

The paper is structured as follows. In Section 2, some fundamentals about matrix Lie groups are given in order to introduce $SE(3)$ and the notations. In Section 3, the beam kinematics in the $SE(3)$ context is worked out. Then, the static and dynamic equilibrium equations are developed in Section 4 and Section 5. The original finite element interpolation formula based on the exponential map of the Lie group is introduced in Section 6 and the discretized strain and velocity fields are also given. The resulting discretized static and dynamic equilibrium equations are developed in Section 7 and Section 8, where a few numerical examples are presented to assess the formulation and enhance some specific features. Finally, some conclusions and perspectives are presented in Section 9.

2. Lie group framework

2.1. Fundamentals about matrix Lie groups

The necessary concepts required for our developments are now introduced. The theoretical concepts are first introduced in a general setting and will then be particularized to the groups $SO(3)$ and $SE(3)$. Explicit expressions useful for computational purposes are given in Appendix A. For a more detailed introduction to Lie groups see, e.g., [16,26,27].

A group G is a set of elements with a composition rule, that associates an element of the group to two elements of the group: if $q_1, q_2 \in G$, then $q_1 \circ q_2 = q_3 \in G$. In the present case, we consider matrix groups and the composition rule is the matrix product written as $q_1 q_2 = q_3$. This composition rule needs to satisfy several properties, e.g. the existence of a neutral element e ($qe = eq = q$), which is simply the identity matrix, and the existence of an inverse ($\forall q \in G,\ \exists!\ q^{-1} :\ qq^{-1} = q^{-1}q = e$). It follows that the elements of such a matrix group are square and invertible matrices. A matrix Lie group is a continuous matrix group for which the composition rule and the inverse are smooth. Therefore, a matrix Lie group is, geometrically speaking, a differentiable manifold, and differential geometry can be used to perform operations on the group.

The tangent space at $q \in G$ is denoted T_qG. In particular, the tangent space at the identity of a Lie group is called the Lie algebra $\mathfrak{g}$ and it is isomorphic to $\mathbb{R}^k$ through the invertible linear map

$$\widetilde{(\bullet)} : \mathbb{R}^k \to \mathfrak{g}, \quad \mathbf{x} \mapsto \widetilde{\mathbf{x}}$$

The composition rule of the Lie group allows the introduction of a left invariant vector field as

$$\delta q = q\widetilde{\delta\mathbf{q}} \tag{1}$$

where $\delta(\bullet)$ means an arbitrary infinitesimal variation of the argument, and δq is thus an arbitrary element belonging to T_qG. Notice the difference in the two following notations: $\widetilde{\delta\mathbf{q}}$ and $\delta(\widetilde{\mathbf{q}})$. The former indicates an infinitesimal increment belonging to the Lie algebra, while the latter means the variation of an element $\widetilde{\mathbf{q}}$ of the Lie algebra. Similarly, $\delta\mathbf{q}$ and $\delta(\mathbf{q})$ stand for the associated expressions in $\mathbb{R}^k$ of respectively the former and the latter notation.

The adjoint representation of a Lie algebra element $\widetilde{\delta\mathbf{q}}$ is defined as

$$\mathrm{Ad}_q(\widetilde{\delta\mathbf{q}}) = q\widetilde{\delta\mathbf{q}}q^{-1} \tag{2}$$

where $\mathrm{Ad}_q : \mathfrak{g} \to \mathfrak{g}$ is a linear map. In this paper, with a slight abuse of notations, Ad_q is also used for the adjoint representation as a linear map acting on $\mathbb{R}^k$ isomorphic elements of the Lie algebra, that is $\mathrm{Ad}_q : \mathbb{R}^k \to \mathbb{R}^k$.

The derivative of q with respect to any parameter $s \in \mathbb{R}$ is written as

$$\frac{dq}{ds} = q\widetilde{\mathbf{u}} \tag{3}$$

where $\widetilde{\mathbf{u}}$ is an element of the Lie algebra. In general, derivatives do not commute and derivatives are related by the compatibility equation

$$\delta(\widetilde{\mathbf{u}}) = \frac{d(\widetilde{\delta\mathbf{q}})}{ds} + [\widetilde{\mathbf{u}}, \widetilde{\delta\mathbf{q}}] \tag{4}$$

where $[\widetilde{\mathbf{a}}, \widetilde{\mathbf{b}}] = \widetilde{\mathbf{a}}\widetilde{\mathbf{b}} - \widetilde{\mathbf{b}}\widetilde{\mathbf{a}} = -[\widetilde{\mathbf{b}}, \widetilde{\mathbf{a}}]$ defines the Lie bracket operator $[\bullet, \bullet]$. Eq. (4) can be written in terms of vectors in $\mathbb{R}^k$ as

$$\delta(\mathbf{u}) = \frac{d(\delta\mathbf{q})}{ds} + \widehat{\mathbf{u}}\delta\mathbf{q} \tag{5}$$

where $\widehat{\bullet}$ is a linear operator which maps a vector in $\mathbb{R}^k$ into a $k \times k$ matrix. In the literature, the $\widehat{\bullet}$ operator is often defined as an adjoint representation and denoted $\mathrm{ad}_{\mathbf{a}}(\mathbf{b}) = \widehat{\mathbf{a}}\mathbf{b}$.

For a given vector field $\widetilde{\mathbf{u}}$, Eq. (3) can be seen as a differential equation on the Lie group. If $\widetilde{\mathbf{u}}$ does not depend on s, the solution is

$$q(s) = q_0 \exp(\widetilde{\mathbf{u}}s)$$

where $q_0 = q(0)$ and exp is the exponential operator, which maps an element of the Lie algebra to an element of the Lie group

$$\exp : \mathfrak{g} \to G, \quad \widetilde{\mathbf{x}} \mapsto \exp(\widetilde{\mathbf{x}})$$

Since the Lie algebra is isomorphic to $\mathbb{R}^k$, the exponential map introduces a local parameterization of the Lie group around any $q_0 \in G$. Indeed, any $q \in G$ may be represented as a function of $\widetilde{\mathbf{x}} \in \mathfrak{g}$ using the exponential operator and the composition with q_0 according to

$$q = q_0 \exp(\widetilde{\mathbf{x}}) \tag{6}$$

By extension, the notation $\exp(\mathbf{x})$ with $\mathbf{x} \in \mathbb{R}^k$ shall be used equivalently since the Lie algebra is isomorphic to $\mathbb{R}^k$. Considering the derivatives, a relationship exists between $\widetilde{\mathbf{u}}$ involved in Eq. (3) and the derivative of $\widetilde{\mathbf{x}}$ defined by the exponential map representation in Eq. (6). It can be expressed as a linear relationship from $\mathbb{R}^k$ to $\mathbb{R}^k$

$$\mathbf{u} = \mathbf{T}(\mathbf{x})\frac{d\mathbf{x}}{ds} \tag{7}$$

where $\mathbf{T}(\mathbf{x})$ is the tangent application of the exponential map. Likewise, we can write $\delta\mathbf{q} = \mathbf{T}(\mathbf{x})\delta\mathbf{x}$. The inverse map of the exponential map is called the logarithmic map such that

$$\log : G \to \mathfrak{g}, \quad q \mapsto \log(q) \tag{8}$$

It is thus a mapping from the Lie group to the Lie algebra, i.e. $\log(q) = \widetilde{\mathbf{x}}$. By extension, the notation $\log(q) = \mathbf{x}$ with $\mathbf{x} \in \mathbb{R}^k$ shall be used equivalently since the Lie algebra is isomorphic to $\mathbb{R}^k$.

Next, two Lie groups of interest are introduced. The group and algebra structures are presented. Explicit formulas for numerical computations can be found in Appendix A.

2.2. The special orthogonal group, $SO(3)$

The special orthogonal group, $SO(3)$, is a matrix Lie group that can be represented by 3×3 proper orthogonal matrices $\mathbf{R}$. In particular, rotation matrices are orthogonal matrices. The neutral element is the 3×3 identity matrix, denoted $\mathbf{I}_{3\times3}$, and the inverse of an element $\mathbf{R} \in SO(3)$ is $\mathbf{R}^T \in SO(3)$, where $\bullet^T$ is the matrix transpose. The composition rule is the matrix product of two 3×3 orthogonal matrices. The Lie algebra, $\mathfrak{so}(3)$, is the space of skew-symmetric matrices and is isomorphic to $\mathbb{R}^3$

$$\boldsymbol{\Omega} = \begin{bmatrix} \Omega_1 \\ \Omega_2 \\ \Omega_3 \end{bmatrix} \in \mathbb{R}^3 \text{ and } \widetilde{\boldsymbol{\Omega}} = \begin{bmatrix} 0 & -\Omega_3 & \Omega_2 \\ \Omega_3 & 0 & -\Omega_1 \\ -\Omega_2 & \Omega_1 & 0 \end{bmatrix} \in \mathfrak{so}(3) \tag{9}$$

In particular, Eq. (1) reads

$$\delta\mathbf{R} = \mathbf{R}\widetilde{\delta\boldsymbol{\Omega}} \tag{10}$$

The $\widehat{\bullet}$ operator defined at Eq. (5) is equivalent to $\widetilde{\bullet}$.

2.3. The special Euclidean group, $SE(3)$

The matrix Lie group $SE(3)$ is the group of Euclidean transformations $\mathbf{H} = \mathcal{H}(\mathbf{R}, \mathbf{x})$ combining a rotation $\mathbf{R} \in SO(3)$ and a vector $\mathbf{x} \in \mathbb{R}^3$. It can be represented by 4×4 matrices

$$\mathbf{H} = \begin{bmatrix} \mathbf{R} & \mathbf{x} \\ \mathbf{0}_{1\times 3} & 1 \end{bmatrix} \tag{11}$$

The neutral element is $\mathbf{I}_{4\times 4}$ and the inverse of $\mathbf{H} \in SE(3)$ is $\mathbf{H}^{-1} \in SE(3)$ given by $\mathbf{H}^{-1} = \mathcal{H}(\mathbf{R}^T, -\mathbf{R}^T\mathbf{x})$, i.e.

$$\mathbf{H}^{-1} = \begin{bmatrix} \mathbf{R}^T & -\mathbf{R}^T\mathbf{x} \\ \mathbf{0}_{1\times 3} & 1 \end{bmatrix} \tag{12}$$

The composition rule is the matrix product of 4×4 matrices. The Lie algebra, denoted $\mathfrak{se}(3)$, is the space of 4×4 matrices $\widetilde{\mathbf{h}}$ as in Eq. (13) and is isomorphic to $\mathbb{R}^6$

$$\mathbf{h} = \begin{bmatrix} \mathbf{h}_U \\ \mathbf{h}_\Omega \end{bmatrix} \in \mathbb{R}^6 \text{ and } \widetilde{\mathbf{h}} = \begin{bmatrix} \widetilde{\mathbf{h}}_\Omega & \mathbf{h}_U \\ \mathbf{0}_{1\times 3} & 0 \end{bmatrix} \in \mathfrak{se}(3) \tag{13}$$

where $\widetilde{\mathbf{h}}_\Omega \in \mathfrak{so}(3)$ and $\mathbf{h}_U \in \mathbb{R}^3$. It is clear from the argument whether the tilde operator denotes the mapping to $\mathfrak{so}(3)$ or $\mathfrak{se}(3)$. Eq. (1) reads

$$\delta\mathbf{H} = \mathbf{H}\widetilde{\delta\mathbf{h}} \Longleftrightarrow \begin{bmatrix} \delta\mathbf{R} & \delta\mathbf{x} \\ \mathbf{0}_{1\times 3} & 0 \end{bmatrix} = \begin{bmatrix} \mathbf{R} & \mathbf{x} \\ \mathbf{0}_{1\times 3} & 1 \end{bmatrix} \begin{bmatrix} \widetilde{\delta\mathbf{h}}_\Omega & \delta\mathbf{h}_U \\ \mathbf{0}_{1\times 3} & 0 \end{bmatrix} \tag{14}$$

in which $\widetilde{\delta\mathbf{h}}_\Omega = \mathbf{R}^T\delta\mathbf{R}$ and $\delta\mathbf{h}_U = \mathbf{R}^T\delta\mathbf{x}$. Accordingly, one has $\delta\mathbf{h} = \begin{bmatrix} \delta\mathbf{h}_U^T & \delta\mathbf{h}_\Omega^T \end{bmatrix}^T \in \mathbb{R}^6$. The $\widehat{\bullet}$ operator defined at Eq. (5) is

$$\widehat{\mathbf{h}} = \begin{bmatrix} \widetilde{\mathbf{h}}_\Omega & \widetilde{\mathbf{h}}_U \\ \mathbf{0}_{3\times 3} & \widetilde{\mathbf{h}}_\Omega \end{bmatrix} \tag{15}$$

Notice that $\widehat{\mathbf{h}}_1\mathbf{h}_2 = -\widehat{\mathbf{h}}_2\mathbf{h}_1$. Let us also define the check operator $\check{\bullet}$ as $\widehat{\mathbf{h}}_1^T\mathbf{h}_2 = \check{\mathbf{h}}_2^T\mathbf{h}_1$, that is

$$\check{\mathbf{h}} = \begin{bmatrix} \mathbf{0}_{3\times 3} & \widetilde{\mathbf{h}}_U \\ \widetilde{\mathbf{h}}_U & \widetilde{\mathbf{h}}_\Omega \end{bmatrix} \tag{16}$$

Based on the Lie group formalism of this section, the rest of the paper addresses the formulation of a beam finite element on $SE(3)$ relying on an original non-linear interpolation method.

3. Beam kinematics

Let us define $s \in [0, L]$ as the spatial parameter along the neutral axis of a beam of length L. $\mathbf{x}^0(s)$ is the position vector of a point of the neutral axis in the reference configuration. Thus, the position of any point p of the beam in the reference configuration can be written as

$$\mathbf{x}_p^0(s,t,u) = \mathbf{x}^0(s) + t\mathbf{i}_t + u\mathbf{i}_u \tag{17}$$

where $\mathbf{i}_t$ and $\mathbf{i}_u$ are the unit vectors of principal axes of the cross-sections in the reference configuration, and t and u are the coordinates along these axes. We assume that the principal axes are constant along the neutral axis. For a beam which is initially straight, $\mathbf{x}^0(s) = s\mathbf{i}_s$, where $\mathbf{i}_s$ is the unit vector along the neutral axis. Then, we introduce the following notation

$$\mathbf{x}_p^0(s,t,u) = \mathbf{x}^0(s) + \mathbf{O}_0\mathbf{y}(t,u) \tag{18}$$

in which $\mathbf{y}(t,u) = [\,0 \quad t \quad u\,]^T$ and $\mathbf{O}_0 = [\,\mathbf{i}_s \quad \mathbf{i}_t \quad \mathbf{i}_u\,]$. $\mathbf{O}_0$ is a constant rotation matrix that accounts for the orientation of the beam in the reference configuration with respect to the inertial frame. We assume that the cross-sections remain undeformed, which means that $\mathbf{y}(t,u)$ is defined from the reference configuration. By extension, the position of a point p in the current configuration can be written as

$$\mathbf{x}_p(s,t,u) = \mathbf{x}(s) + \mathbf{R}(s)\mathbf{O}_0\mathbf{y}(t,u) \tag{19}$$

where $\mathbf{x}(s)$ is the position vector of the neutral axis and $\mathbf{R}(s)$ characterizes the rotation of the cross-section. The description is illustrated in Fig. 1.

In the $SE(3)$ formalism, a material frame is attached to any material point. The material frame at any point on the neutral axis of the beam is described by a mapping $\mathbb{R} \to SE(3) : s \mapsto \mathbf{H}(s)$ and is therefore represented by $\mathbf{H}(s) = \mathcal{H}(\mathbf{I}_{3\times 3}, \mathbf{x}^0(s))$ in the

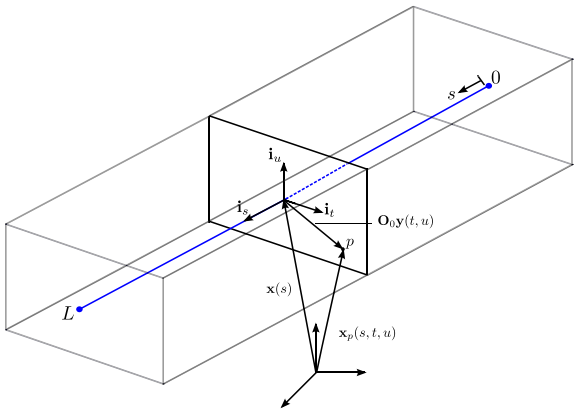

Fig. 1. Description of the beam kinematics.

reference configuration and $\mathbf{H}(s) = \mathcal{H}(\mathbf{R}(s), \mathbf{x}(s))$ in the current configuration. By construction, this material frame in the reference frame is aligned with the inertial frame and not with the cross-section axes $\mathbf{i}_s, \mathbf{i}_t, \mathbf{i}_u$. Based on Eq. (19), the material frame at any beam point p of coordinates (s,t,u) is related to the material frame attached to the neutral axis by the frame transformation

$$\mathbf{H}_p(s,t,u) = \mathbf{H}(s)\begin{bmatrix} \mathbf{I}_{3\times 3} & \mathbf{O}_0\mathbf{y}(t,u) \\ \mathbf{0}_{1\times 3} & 1 \end{bmatrix} = \mathbf{H}(s)\mathbf{H}_{\mathbf{y}}(t,u) \tag{20}$$

where $\mathbf{H}_p(s,t,u) = \mathcal{H}(\mathbf{R}_p(s), \mathbf{x}_p(s,t,u))$. According to the assumption that the cross-sections remain straight, $\mathbf{H}_{\mathbf{y}}(t,u)$ is defined from the reference configuration and $\mathbf{R}_p(s) = \mathbf{R}(s)$.

4. Static formulation

4.1. Deformation field

The deformations of the neutral axis are introduced from the deformation gradient of the material frame on the neutral axis. Owing to the Lie group derivative in Eq. (3), the deformation gradient is a Lie algebra element denoted as $\widetilde{\mathbf{f}} \in \mathfrak{se}(3)$ and is defined from

$$\frac{d\mathbf{H}(s)}{ds} = \mathbf{H}(s)\widetilde{\mathbf{f}} \tag{21}$$

where $\mathbf{f} = [\mathbf{f}_U^T \ \mathbf{f}_\Omega^T]^T$. The deformation gradient can be split into

$$\mathbf{f} = \mathbf{f}^0 + \boldsymbol{\epsilon} \tag{22}$$

where $\mathbf{f}^0$ refers to the values in the reference configuration and $\boldsymbol{\epsilon}$ accounts for the deformations of the current configuration with respect to the reference configuration. For an initially straight beam, $\mathbf{f}^{0T} = [\mathbf{i}_s^T \ \mathbf{0}_{3\times 1}^T]^T$. In order to match classical notations for the position part and the rotation part of the deformations, the following notation is introduced

$$\boldsymbol{\epsilon} = \begin{bmatrix} \boldsymbol{\gamma} \\ \boldsymbol{\kappa} \end{bmatrix} \tag{23}$$

Notice that, considering Eq. (23), the deformation measure at the position level reads $\boldsymbol{\gamma} = \mathbf{R}^T(s)\frac{d\mathbf{x}(s)}{ds} - \mathbf{f}_U^0$, which is equivalent to classical deformation measures of the neutral axis in beam element formulation [1]. According to the introduction of $\mathbf{O}_0$ in Eq. (18), the deformation of the neutral axis in the cross-section axes is measured by $\mathbf{O}_0^T\boldsymbol{\gamma}$. In particular, $\mathbf{i}_s^T\boldsymbol{\gamma}$ represents the strain along the neutral axis whereas $\mathbf{i}_t^T\boldsymbol{\gamma}$ and $\mathbf{i}_u^T\boldsymbol{\gamma}$ represent the shear strains along the cross-section axes $\mathbf{i}_u$ and $\mathbf{i}_t$ respectively.

The deformations at any point of the cross-sections are obtained from the derivative of the material frame in (20) with respect to s, which leads to

$$\frac{\partial\mathbf{H}_p(s,t,u)}{\partial s} = \mathbf{H}_p(s,t,u)\widetilde{\mathbf{f}}_p \tag{24}$$

in which $\widetilde{\mathbf{f}}_p = \mathbf{H}_{\mathbf{y}}^{-1}\widetilde{\mathbf{f}}\mathbf{H}_{\mathbf{y}} = \mathrm{Ad}_{\mathbf{H}_{\mathbf{y}}^{-1}}(\widetilde{\mathbf{f}})$. Similarly to Eqs. (22) and (23), the deformation gradient can be split into $\mathbf{f}_p = \mathbf{f}_p^0 + \boldsymbol{\epsilon}_p$ where

$$\mathbf{f}_p = \begin{bmatrix} \mathbf{f}_{pU} \\ \mathbf{f}_\Omega \end{bmatrix}; \boldsymbol{\epsilon}_p = \begin{bmatrix} \boldsymbol{\gamma}_p \\ \boldsymbol{\kappa} \end{bmatrix} \tag{25}$$

in which $\mathbf{f}_{pU} = \mathbf{f}_U - \widetilde{\mathbf{O}_0\mathbf{y}}\mathbf{f}_\Omega$ and

$$\boldsymbol{\gamma}_p = \mathbf{f}_{pU} - \mathbf{f}^0_{pU} = \boldsymbol{\gamma} - \widetilde{\mathbf{O}_0\mathbf{y}}\boldsymbol{\kappa} \tag{26}$$

Therefore, $\boldsymbol{\kappa}$ is interpreted as a vector of curvatures. They can be interpreted in the cross-section axes by considering $\mathbf{O}_0^T\boldsymbol{\kappa}$. In particular, $\mathbf{i}_s^T\boldsymbol{\kappa}$ represents the torsion about the neutral axis whereas $\mathbf{i}_t^T\boldsymbol{\kappa}$ and $\mathbf{i}_u^T\boldsymbol{\kappa}$ represent the bending curvatures about the cross-section axes $\mathbf{i}_u$ and $\mathbf{i}_t$ respectively.

Let us now consider the metric tensors to build the deformation tensor. $\mathbf{g}$, the metric tensor in the deformed configuration, is defined as

$$\mathbf{g}_{ij} = \left(\frac{\partial \mathbf{x}_p(s,t,u)}{\partial x_i}\right)^T \frac{\partial \mathbf{x}_p(s,t,u)}{\partial x_j} \tag{27}$$

with $x_i, x_j = \{s,t,u\}$. Using Eqs. (19) and (25), the partial derivatives are given by

$$\frac{\partial \mathbf{x}_p(s,t,u)}{\partial s} = \mathbf{R}(s)\mathbf{f}_{pU}; \quad \frac{\partial \mathbf{x}_p(s,t,u)}{\partial t} = \mathbf{R}(s)\mathbf{i}_t; \quad \frac{\partial \mathbf{x}_p(s,t,u)}{\partial u} = \mathbf{R}(s)\mathbf{i}_u \tag{28}$$

Notice that each derivative involves a rotation matrix multiplied by a vector evaluated in the reference configuration, leading to a natural polar decomposition of the deformation gradient. The metric tensor in the reference configuration, denoted $\mathbf{g}^0$, has the same definition as $\mathbf{g}$, but involves $\mathbf{x}^0_p, \mathbf{f}^0_{pU}$ and $\mathbf{R}(s) = \mathbf{I}_{3\times3}$. Notice that due to the assumption that the cross-sections remain undeformed, $\mathbf{i}_t$ and $\mathbf{i}_u$ are defined from the reference configuration and do not depend on the deformation state of the beam.

The Green–Lagrange strain tensor $\mathbf{GL}_{ij} = \frac{1}{2}(\mathbf{g}_{ij} - \mathbf{g}^0_{ij})$ can now be computed. It involves three kinds of terms

$$\mathbf{GL}_{ss} = \boldsymbol{\gamma}_p^T\mathbf{f}^0_{pU} + \frac{1}{2}\boldsymbol{\gamma}_p^T\boldsymbol{\gamma}_p; \quad \mathbf{GL}_{si} = \frac{1}{2}\boldsymbol{\gamma}_p^T\mathbf{i}_i; \quad \mathbf{GL}_{ij} = 0 \tag{29}$$

with $i,j = \{t,u\}$. Assuming that the deformations $\boldsymbol{\gamma}$ and $\boldsymbol{\kappa}$ are small, the second order term $\boldsymbol{\gamma}_p^T\boldsymbol{\gamma}_p$ in $\mathbf{GL}_{ss}$ can be neglected. This classical assumption is used throughout this paper in order to simplify the developments, although the extension to the large deformation case can be carried out straightforwardly following the same strategy.

4.2. Strain energy

Based on the Green–Lagrange strain tensor, the strain energy can be computed as

$$\mathcal{W}_{int} = \frac{1}{2}\int_V \mathbf{S} : \mathbf{GL}\, dV = \frac{1}{2}\int_V \boldsymbol{\gamma}_p^T(\mathbf{S}_{ss}\mathbf{f}^0_{pU} + \mathbf{S}_{st}\mathbf{i}_t + \mathbf{S}_{su}\mathbf{i}_u)\, dV \tag{30}$$

where $\mathbf{S}$ is the second Piola–Kirchhoff stress tensor and V is the volume of the beam in the reference configuration. Using Eq. (26) and owing to the fact that $\boldsymbol{\gamma}$ and $\boldsymbol{\kappa}$ do not depend on t and u, the integral over the cross-sections can be computed, which leads to

$$\mathcal{W}_{int} = \frac{1}{2}\int_0^L (\boldsymbol{\gamma}^T\mathbf{n} + \boldsymbol{\kappa}^T\mathbf{m})\, ds \tag{31}$$

where $\mathbf{n}$ and $\mathbf{m}$ are respectively the resulting forces and moments over the cross-sections defined as

$$\mathbf{n} = \int_A (\mathbf{S}_{ss}\mathbf{f}^0_{pU} + \mathbf{S}_{st}\mathbf{i}_t + \mathbf{S}_{su}\mathbf{i}_u)\, dA \tag{32}$$

$$\mathbf{m} = \int_A \widetilde{\mathbf{O}_0\mathbf{y}}(\mathbf{S}_{ss}\mathbf{f}^0_{pU} + \mathbf{S}_{st}\mathbf{i}_t + \mathbf{S}_{su}\mathbf{i}_u)\, dA \tag{33}$$

The expression of the resulting forces and moments in the cross-section axes are obtained by premultiplying $\mathbf{n}$ and $\mathbf{m}$ by $\mathbf{O}_0^T$, according to Eq. (18). In particular, $\mathbf{i}_s^T\mathbf{n}$ is the force along the neutral axis, and $\mathbf{i}_t^T\mathbf{n}$ and $\mathbf{i}_u^T\mathbf{n}$ are the shear forces along the cross-section axes $\mathbf{i}_t$ and $\mathbf{i}_u$ respectively. Similarly, $\mathbf{i}_s^T\mathbf{m}$ is the torsion moment about the neutral axis, and $\mathbf{i}_t^T\mathbf{m}$ and $\mathbf{i}_u^T\mathbf{m}$ are the bending moments about the cross-section axes $\mathbf{i}_t$ and $\mathbf{i}_u$ respectively. For a linear elastic material, the constitutive law provides a linear relationship between the cross-section resultants and the deformations

$$\begin{bmatrix} \mathbf{n} \\ \mathbf{m} \end{bmatrix} = \underbrace{\begin{bmatrix} \mathbf{K}_U & \mathbf{0}_{3\times3} \\ \mathbf{0}_{3\times3} & \mathbf{K}_\Omega \end{bmatrix}}_{=\mathbf{K}} \begin{bmatrix} \boldsymbol{\gamma} \\ \boldsymbol{\kappa} \end{bmatrix} \tag{34}$$

where $\mathbf{K}$ contains the usual stiffness parameters. In simple cases, it is diagonal and $\mathbf{K}_U = \mathbf{O}_0\mathrm{diag}(EA, GA_t, GA_u)\mathbf{O}_0^T$ contains the axial and shear stiffnesses whereas $\mathbf{K}_\Omega = \mathbf{O}_0\mathrm{diag}(GJ, EI_t, EI_u)\mathbf{O}_0^T$ contains the torsional and bending stiffnesses. Notice that the

effect of $\mathbf{O}_0$ is to express in the material frame the stiffnesses, which are originally computed in the cross-section axes namely in the $\mathbf{i}_s, \mathbf{i}_t, \mathbf{i}_u$ frame. Eventually, the strain energy can be written as

$$\mathcal{W}_{int} = \frac{1}{2}\int_0^L \boldsymbol{\epsilon}^T \mathbf{K} \boldsymbol{\epsilon}\, ds \tag{35}$$

4.3. Static equilibrium equation

The virtual work principle states that equilibrium is achieved when

$$\delta(\mathcal{W}_{int}) = \delta(\mathcal{W}_{ext}) \tag{36}$$

Starting from Eq. (35), the variation of the strain energy is given by

$$\delta(\mathcal{W}_{int}) = \int_0^L \delta(\boldsymbol{\epsilon})^T \mathbf{K} \boldsymbol{\epsilon}\, ds \tag{37}$$

Due to the Lie group framework, the variation of the deformation is related to the variation of the state variables, which are $SE(3)$ elements, as in Eq. (5). According to the definitions in Eq. (21) and in Eq. (22), it is given by

$$\delta(\boldsymbol{\epsilon}) = \delta(\mathbf{f}) = \frac{d}{ds}(\delta\mathbf{h}) + \hat{\mathbf{f}}^T \delta\mathbf{h} \tag{38}$$

in which $\widetilde{\delta\mathbf{h}} = \mathbf{H}^{-1}\delta\mathbf{H}$. Inserting Eq. (38) into Eq. (37) and integrating by parts yields

$$\delta(\mathcal{W}_{int}) = \left[\delta\mathbf{h}^T \mathbf{K}\boldsymbol{\epsilon}\right]_0^L - \int_0^L \delta\mathbf{h}^T \left(\mathbf{K}\frac{d}{ds}(\boldsymbol{\epsilon}) - \hat{\mathbf{f}}^T \mathbf{K}\boldsymbol{\epsilon}\right) ds \tag{39}$$

where the first term is interpreted as a boundary condition term.

In general, the virtual work done by external forces can be written as

$$\delta(\mathcal{W}_{ext}) = \int_0^L \delta\mathbf{h}^T \mathbf{g}_{ext}\, ds \tag{40}$$

where $\mathbf{g}_{ext}$ contain the resulting forces and moments over the cross-sections due to an external loading. Notice that the external forces must be expressed in the material frame, that is, pulled back from the inertial frame.

Finally, the weak form of the equilibrium equation is obtained by inserting Eqs. (39) and (40) into Eq. (36), which yields

$$\left[\delta\mathbf{h}^T \mathbf{K}\boldsymbol{\epsilon}\right]_0^L - \int_0^L \delta\mathbf{h}^T \left(\mathbf{K}\frac{d}{ds}(\boldsymbol{\epsilon}) - \hat{\mathbf{f}}^T \mathbf{K}\boldsymbol{\epsilon} + \mathbf{g}_{ext}\right) ds = 0 \tag{41}$$

Accordingly, the strong form of the equilibrium equation is then obtained as a six-dimensional non-linear ordinary differential equation for the unknown $\boldsymbol{\epsilon}$

$$\mathbf{K}\frac{d}{ds}(\boldsymbol{\epsilon}) - \hat{\mathbf{f}}^T \mathbf{K}\boldsymbol{\epsilon} + \mathbf{g}_{ext} = \mathbf{0} \tag{42}$$

It is interesting to notice that the homogeneous equation does not involve the position nor the orientation of the beam. It is a direct consequence of the present framework, namely the equations are written in the material frame. Thus, if the external forces do not depend on the state of the beam, Eqs. (42) and (21) are uncoupled, and the state of the beam can be recovered from Eq. (21) once Eq. (42) is solved. However, in general, the external forces may depend on the state of the beam. In this case, Eq. (21) must be solved together with Eq. (42).

5. Dynamic formulation

5.1. Velocity field

The velocity field of a point of the neutral axis is introduced by the Lie algebra element $\widetilde{\mathbf{v}}$ related to the time derivative of $\mathbf{H}(s)$

$$\dot{\mathbf{H}}(s) = \mathbf{H}(s)\widetilde{\mathbf{v}} \tag{43}$$

where $\mathbf{v} = \begin{bmatrix}\mathbf{v}_U^T & \mathbf{v}_\Omega^T\end{bmatrix}^T$. Remembering the nature of the Lie algebra element of $SE(3)$ in Eq. (14), the velocities $\mathbf{v}$ are expressed in the material frame. According to Eq. (18), the velocity of the neutral axis in the cross-section axes are measured by $\mathbf{O}_0^T\mathbf{v}_U$. In particular, $\mathbf{i}_s^T\mathbf{v}_U$ represents the velocity along the neutral axis whereas $\mathbf{i}_t^T\mathbf{v}_U$ and $\mathbf{i}_u^T\mathbf{v}_U$ represent the velocities along the cross-section axes $\mathbf{i}_u$ and $\mathbf{i}_t$ respectively. The rotation part $\mathbf{v}_\Omega$ can also be interpreted in the cross-section axes. In particular, $\mathbf{i}_s^T\mathbf{v}_\Omega, \mathbf{i}_t^T\mathbf{v}_\Omega$ and $\mathbf{i}_u^T\mathbf{v}_\Omega$ represent the rotation velocities about $\mathbf{i}_s, \mathbf{i}_u$ and $\mathbf{i}_t$ respectively.

Observing that $\mathbf{H_y}$ is a constant matrix, the velocities at any point of the cross-sections can be computed from the time derivative of the material frame in (20), which leads to

$$\dot{\mathbf{H}}_p(s,t,u) = \mathbf{H}_p(s,t,u)\widetilde{\mathbf{v}}_p \tag{44}$$

in which $\widetilde{\mathbf{v}}_p = \mathbf{H}_{\mathbf{y}}^{-1}\widetilde{\mathbf{v}}\mathbf{H}_{\mathbf{y}} = \mathrm{Ad}_{\mathbf{H}_y^{-1}}(\widetilde{\mathbf{v}})$, so that

$$\mathbf{v}_p = \begin{bmatrix} \mathbf{v}_{pU} \\ \mathbf{v}_\Omega \end{bmatrix} \tag{45}$$

where $\mathbf{v}_{pU} = \mathbf{v}_U - \widetilde{\mathbf{O_0 y}}\mathbf{v}_\Omega$.

5.2. Kinetic energy

Denoting ρ the mass density of the material, the kinetic energy $\mathcal{K}$ is given by

$$\mathcal{K} = \frac{1}{2}\int_V \rho \mathbf{v}_{Up}^T \mathbf{v}_{Up}\, dV = \frac{1}{2}\int_0^L \mathbf{v}^T \mathbf{M}_C \mathbf{v}\, ds \tag{46}$$

in which $\mathbf{M}_C$ contains the usual mass and rotation inertia properties of the cross-sections

$$\mathbf{M}_C = \int_A \rho \begin{bmatrix} \mathbf{I}_{3\times 3} & -\widetilde{\mathbf{O_0 y}} \\ \widetilde{\mathbf{O_0 y}} & -\widetilde{\mathbf{O_0 y}}\widetilde{\mathbf{O_0 y}} \end{bmatrix} dA = \begin{bmatrix} \frac{m}{L}\mathbf{I}_{3\times 3} & -\mathbf{O_0 J}_I \mathbf{O}_0^T \\ -\mathbf{O_0 J}_I^T \mathbf{O}_0^T & \mathbf{O_0 J O}_0^T \end{bmatrix} \tag{47}$$

where m is the mass of the element, and $\mathbf{J}_I$ and $\mathbf{J}$ are respectively the first and the second moment of inertia of the cross-sections computed in the local axes of the beam, namely the frame defined by $\mathbf{i}_s, \mathbf{i}_t, \mathbf{i}_u$. In most practical cases, $\mathbf{J}_I$ vanishes and $\mathbf{J}$ is diagonal. Since the cross-sections are assumed to be undeformable, $\mathbf{M}_C$ is defined from the reference configuration of the beam and does not depend on the motion of the beam.

5.3. Dynamic equilibrium equation

The dynamic equilibrium equations can be obtained from Hamilton's principle, which states that the action integral over the time interval $[\tau_0, \tau_1]$ is stationary

$$\int_{\tau_0}^{\tau_1} \left(\delta(\mathcal{K}) - \delta(\mathcal{W}_{int}) + \delta(\mathcal{W}_{ext})\right) d\tau = 0 \tag{48}$$

where the variations are fixed at τ_0 and τ_1. The strain energy $\mathcal{W}_{int}$ and the work done by the external forces $\mathcal{W}_{ext}$ were treated in Section 4. From Eq. (46), the variation of the kinetic energy reads

$$\delta(\mathcal{K}) = \int_0^L \delta(\mathbf{v})^T \mathbf{M}_C \mathbf{v}\, ds \tag{49}$$

Due to the Lie group structure, the variation of the velocity in terms of the variation of the state variables is expressed according to Eq. (5), that is

$$\delta(\mathbf{v}) = \frac{d}{d\tau}(\delta\mathbf{h}) + \widehat{\mathbf{v}}\delta\mathbf{h} \tag{50}$$

in which $\widetilde{\delta\mathbf{h}} = \mathbf{H}^{-1}\delta\mathbf{H}$. Inserting this into Eq. (49), we obtain, after integration by parts,

$$\int_{\tau_0}^{\tau_1} \delta(\mathcal{K})\, d\tau = \left[\int_0^L \delta\mathbf{h}^T \mathbf{M}_C \mathbf{v}\, ds\right]_{\tau_0}^{\tau_1} - \int_{\tau_0}^{\tau_1}\int_0^L \delta\mathbf{h}^T(\mathbf{M}_C\dot{\mathbf{v}} - \widehat{\mathbf{v}}^T\mathbf{M}_C\mathbf{v})\, ds\, d\tau \tag{51}$$

Since the variations are fixed at τ_0 and τ_1, the first term on the right hand side vanishes. Combining the latter result with Eq. (41), Eq. (48) yields the following weak form of the dynamic equilibrium equations

$$\left[\delta\mathbf{h}^T\mathbf{K}\boldsymbol{\epsilon}\right]_0^L - \int_0^L \delta\mathbf{h}^T\left(\mathbf{M}_C\dot{\mathbf{v}} - \widehat{\mathbf{v}}^T\mathbf{M}_C\mathbf{v} + \mathbf{K}\frac{d}{ds}(\boldsymbol{\epsilon}) - \hat{\mathbf{f}}^T\mathbf{K}\boldsymbol{\epsilon} + \mathbf{g}_{ext}\right) ds = 0 \tag{52}$$

which provides a six-dimensional non-linear partial differential equation for the unknowns $\boldsymbol{\epsilon}$ and $\mathbf{v}$

$$\mathbf{M}_C\dot{\mathbf{v}} - \widehat{\mathbf{v}}^T\mathbf{M}_C\mathbf{v} + \mathbf{K}\frac{d}{ds}(\boldsymbol{\epsilon}) - \hat{\mathbf{f}}^T\mathbf{K}\boldsymbol{\epsilon} + \mathbf{g}_{ext} = 0 \tag{53}$$

In general, this equation must be solved together with Eqs. (21) and (43). These last two equations lead to a compatibility equation between the second spatial and time derivatives in the Lie group setting (see Eq. (5)) that can be written as

$$\frac{d}{ds}(\mathbf{v}) - \dot{\boldsymbol{\epsilon}} = \widehat{\mathbf{v}}\boldsymbol{\epsilon} \Longleftrightarrow \frac{d}{ds}(\mathbf{v}) - \dot{\boldsymbol{\epsilon}} = -\hat{\boldsymbol{\epsilon}}\mathbf{v} \tag{54}$$

Notice that this compatibility equation does not depend on the state of the beam. Hence, when the external forces do not depend on the beam configuration, it is sufficient to solve Eqs. (53) and (54) together, and the state of the beam can be recovered afterwards either from Eq. (21) or Eq. (43).

6. Finite element discretization

In order to solve the equilibrium equations developed in Eq. (42) and in Eq. (53), we introduce a finite element approximation of the beam which consists thus in the interpolation of $SE(3)$ elements. In this framework, the knowledge of the position and orientation of the nodal values is essential to allow the connection of the elements and express general external forces.

6.1. Non-linear interpolation formula

The spatial discretization along the neutral axis of the beam is introduced by an interpolation with the variable $s \in [0, L]$ between two end nodes A at $s = 0$ and B at $s = L$, where the nodal frames $\mathbf{H}_A$ and $\mathbf{H}_B$ are located. The proposed interpolation formula reads

$$\mathbf{H}(s) = \mathbf{H}_A \exp_{SE(3)}\left(\frac{s}{L}\mathbf{d}\right) \tag{55}$$

where $\mathbf{d} = \begin{bmatrix} \mathbf{d}_U^T & \mathbf{d}_\Omega^T \end{bmatrix}^T$ is called the relative configuration vector and is defined as

$$\mathbf{d} = \log_{SE(3)}(\mathbf{H}_A^{-1}\mathbf{H}_B) \tag{56}$$

The exponential map and the logarithmic map on $SE(3)$ are provided in Eqs. (A.10) and (A.15). Formula (55) can be seen as an extension of classical linear interpolation formula to non-linear spaces. Basically, the use of the exponential map introduces a local parameterization that allows describing the neutral axis between the two nodes A and B with an element belonging to a linear space, that is a Lie algebra element. The description of any material point of a beam is readily obtained by introducing Eq. (55) into Eq. (20).

Notice that $\mathbf{d}$ is invariant under rigid body motions since, for any $\mathbf{H}^*, \mathbf{H}^*\mathbf{H}_A$ and $\mathbf{H}^*\mathbf{H}_B$ correspond to a rigid motion of the beam and lead to the same value of $\mathbf{d}$. Therefore, the interpolation formula automatically satisfies the frame invariance requirement.

In the reference configuration, $\mathbf{H}_A = \mathcal{H}(\mathbf{I}_{3\times3}, \mathbf{x}_A^0)$ and $\mathbf{H}_B = \mathcal{H}(\mathbf{I}_{3\times3}, \mathbf{x}_B^0)$ so that $\mathbf{d}_U^0 = \mathbf{x}_B^0 - \mathbf{x}_A^0$ and $\mathbf{d}_\Omega^0 = \mathbf{0}_{3\times1}$. Hence, it can be observed that $\|\mathbf{d}_U^0\| = L$. The advantage of setting the rotation matrices in the reference configuration to identity matrices is that the connection between nodes is easily achieved, without having to consider the particular orientation of the beam they belong to. However, the information about the orientation of a given element in the reference configuration is used in the evaluation of the element forces, and in particular the evaluation of the stiffness (Eq. (34)) and mass (Eq. (47)) matrices.

6.2. Geometric interpretation

Classical beam theories imply that position and rotation variables are kinematically coupled and the equations of mechanics developed under such kinematic assumptions yield in general coupled differential equations that govern both the position and the rotation variables. For example, in a cantilever beam, the cross-sections rotate under a tip shear load and a tip bending moment produces a displacement of the neutral axis. However, in usual finite element discretization schemes, the position and the rotation variables are treated as independent variables as well as their increments. It is not the case with the proposed formulation. Indeed, the position of a point of the neutral axis computed using the interpolation formula (55) reads

$$\mathbf{x}(s) = \mathbf{x}_A + \mathbf{R}_A \mathbf{T}_{SO(3)}^T\left(\frac{s}{L}\mathbf{d}_\Omega\right)\frac{s}{L}\mathbf{d}_U \tag{57}$$

where both $\mathbf{d}_U$ and $\mathbf{d}_\Omega$ are involved. It means that the coupling between the positions and the rotations is deeper compared to usual formulations. Moreover, the interpolation of the positions in Eq. (57) is non-linear due to the tangent application $\mathbf{T}_{SO(3)}^T$ from the exponential map $\exp_{SE(3)}$. The interpolation of the rotations is also non-linear and reads

$$\mathbf{R}(s) = \mathbf{R}_A \exp_{SO(3)}\left(\frac{s}{L}\mathbf{d}_\Omega\right) \tag{58}$$

which is identical to the formula proposed in [12], namely only the relative rotation is interpolated.

According to Eq. (57), the interpolation method allows the description of a non-linear displacement field. In order to discuss the geometry of the displacement field let us compute the curvature k of the neutral axis using the classical formula

$$k = \left\|\frac{d}{ds}(\mathbf{t}(s))\right\| = \frac{\|\tilde{\mathbf{d}}_\Omega \mathbf{d}_U\|}{\|\mathbf{d}_U\|} \tag{59}$$

since

$$\frac{d}{ds}(\mathbf{t}(s)) = \frac{d}{ds}\left(\frac{d\mathbf{x}}{ds}\left\|\frac{d\mathbf{x}}{ds}\right\|^{-1}\right) = \mathbf{R}(s)\frac{\widetilde{\mathbf{d}}_\Omega \mathbf{d}_U}{\|\mathbf{d}_U\|} \tag{60}$$

where $\mathbf{t}(s)$ is the unit vector which is tangent to the curve. The curvature is thus constant over the element. Therefore, the proposed interpolation method is able to represent exactly an element of constant curvature due to the non-linear coupling between the position and the rotation in Eq. (57). For example, the interpolation method represents the exact displacement of a beam in pure bending since in that case the exact solution is a curve of constant curvature. This would not be possible in formulations based on first order or higher order interpolation of the displacement field independent from the rotation field. Let us consider a planar cantilever beam subjected to a bending moment at its free end. From strength of materials, the solution is known to be a pure bending deformation and a neutral axis of constant curvature. Classical linear interpolation methods for a shear deformable beam element lead to a geometric inconsistency. Indeed, the linear interpolation of the positions means that the element is a straight line (no curvature) but varying cross-section orientations along the neutral axis is a mark of curvature. Adding more elements allows that the collection of straight lines converge towards the actual curve of the neutral axis. Here, we show that the proposed method provides the geometrically exact displacement in pure bending. Let us consider that the beam is initially aligned with the x-axis of the inertial frame in the reference configuration and a moment M is applied about the z-axis (see Fig. 2). The exact displacement field reads

$$x(s) = \frac{1}{k}\sin(sk) \quad y(s) = \frac{1}{k}(1-\cos(sk)) \quad z(s) = 0 \tag{61}$$

where $k = M/(EI)$ is the curvature. In the reference configuration, we have $\mathbf{d}_U^0 = [L\ 0\ 0]^T$ and $\mathbf{d}_\Omega^0 = [0\ 0\ 0]^T$. Since the beam is clamped at the origin, $\mathbf{H}_A = \mathcal{H}(\mathbf{I}_{3\times3}, \mathbf{0}_{3\times1})$. In pure bending, the neutral axis does not undergo any axial or shear deformation so that $\mathbf{d}_U = \mathbf{d}_U^0$, however the neutral axis gets a curvature k in the xy-plane and $\mathbf{d}_\Omega = L[0\ 0\ k]^T$. Introducing these in the non-linear interpolation field in Eq. (57) and considering the exact expression of $\mathbf{T}_{SO(3)}^T$ in Eq. (A.10) turn out to yield the exact solution given in Eq. (61). Since the exact solution of the planar cantilever beam problem is a curve of constant curvature, one single element matches exactly the analytical displacement field.

The relative curvature k that can be represented is limited to the validity of the logarithmic map. For pure bending, $|Lk| < \pi$, this is because the logarithmic map returns a value $\in]-\pi, \pi[$ and does not see a difference between rotations that are separated from each other by a multiple of 2π. Notice that even in general three dimensional cases, pure bending still takes place in a plane, and the discussion of this section remains valid, although the bending was considered here in the xy-plane for conciseness.

Let us mention that the interpolated neutral axis has a constant torsion as well. Further computations of the Frenet's triad would show that the torsion of the neutral axis is given by $-\mathbf{d}_\Omega^T \mathbf{d}_U / \|\mathbf{d}_U\|$. These observations indicate a close connection of the proposed interpolation with the helicoidal shape functions proposed in [13], where one of the starting ideas was precisely to design constant curvature elements.

6.3. Strain and velocity discretization

Firstly, let us consider the derivatives of Eq. (55) with respect to s

$$\frac{d\mathbf{H}(s)}{ds} = \mathbf{H}(s)\left(\mathbf{T}_{SE(3)}\left(\frac{s}{L}\mathbf{d}\right)\frac{\mathbf{d}}{L}\right)^{\sim} = \mathbf{H}(s)\frac{\widetilde{\mathbf{d}}}{L} \tag{62}$$

where the second equality is straightforwardly obtained by considering $(\widehat{\mathbf{d}})^i \mathbf{d} = \mathbf{0}, \forall i$ and the series development of the tangent operator (see Eq. (A.2)). By comparison with Eq. (21), the discretized expression of the deformation gradient $\mathbf{f}$ is obtained as

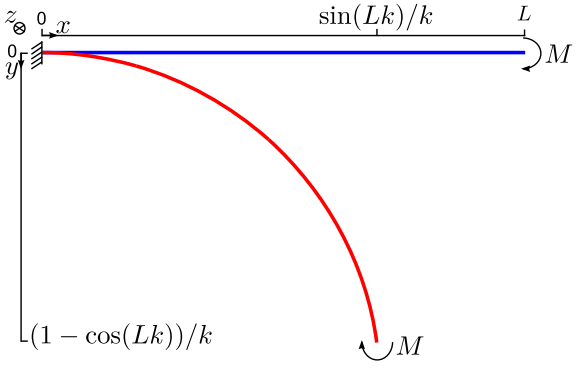

Fig. 2. Cantilever beam subjected to a moment M at its free end. The reference configuration is initially horizontal and the deformed configuration is a planar curve of constant curvature.

$$\mathbf{f} = \frac{\mathbf{d}}{L} \tag{63}$$

It appears then that the Lie algebra element associated with the space derivative is constant. Hence, the deformation, which is measured in the material frame, is also constant over the element and, using Eq. (22), is given by

$$\boldsymbol{\epsilon} = \frac{\mathbf{d} - \mathbf{d}^0}{L} \tag{64}$$

For later use, let us compute the variation of $\mathbf{d}$. It is obtained by taking the variation of Eq. (56) and, introducing a 12×1 virtual increment vector $\delta\mathbf{h}_{AB} = \begin{bmatrix} \delta\mathbf{h}_A^T & \delta\mathbf{h}_B^T \end{bmatrix}^T$ from the variation of the nodal values $\delta\mathbf{H}_A = \mathbf{H}_A\widetilde{\delta\mathbf{h}}_A$ and $\delta\mathbf{H}_B = \mathbf{H}_B\widetilde{\delta\mathbf{h}}_B$, we have

$$\delta(\mathbf{d}) = \mathbf{P}(\mathbf{d})\delta\mathbf{h}_{AB} \tag{65}$$

where

$$\mathbf{P}(\mathbf{d}) = \begin{bmatrix} -\mathbf{T}_{SE(3)}^{-1}(-\mathbf{d}) & \mathbf{T}_{SE(3)}^{-1}(\mathbf{d}) \end{bmatrix} \tag{66}$$

Secondly, the variation of the interpolated field, that is $\delta\mathbf{H}(s) = \mathbf{H}(s)\widetilde{\delta\mathbf{h}}$, can be expressed in terms of the variation of the nodal values. The variation of Eq. (55) reads

$$\delta\mathbf{H}(s) = \mathbf{H}(s)\left(\mathrm{Ad}_{\exp_{SE(3)}\left(\frac{s}{L}\mathbf{d}\right)}\delta\mathbf{h}_A + \frac{s}{L}\mathbf{T}_{SE(3)}\left(\frac{s}{L}\mathbf{d}\right)\delta(\mathbf{d})\right)^{\sim} \tag{67}$$

Using Eq. (65) and the following identity, which can be easily proved using the series developments given in Appendix A,

$$\mathrm{Ad}_{\exp_{SE(3)}\left(-\frac{s}{L}\mathbf{d}\right)} + \frac{s}{L}\mathbf{T}_{SE(3)}\left(\frac{s}{L}\mathbf{d}\right)\left(\mathbf{T}_{SE(3)}^{-1}(\mathbf{d}) - \mathbf{T}_{SE(3)}^{-1}(-\mathbf{d})\right) = \mathbf{I}_{6\times 6} \tag{68}$$

the discretization is given by

$$\delta\mathbf{h} = \mathbf{Q}(s,\mathbf{d})\delta\mathbf{h}_{AB} \tag{69}$$

where

$$\mathbf{Q}(s,\mathbf{d}) = \begin{bmatrix} \mathbf{I}_{6\times 6} - \mathbf{T}^*(s,\mathbf{d}) & \mathbf{T}^*(s,\mathbf{d}) \end{bmatrix} \tag{70}$$

and $\mathbf{T}^* = (s/L)\ \mathbf{T}_{SE(3)}(s\mathbf{d}/L)\ \mathbf{T}_{SE(3)}^{-1}(\mathbf{d})$.

Thirdly, regarding the velocity field, the same process as for the variation can be conducted such that

$$\mathbf{v} = \mathbf{Q}(s,\mathbf{d})\mathbf{v}_{AB} \tag{71}$$

where a 12×1 velocity vector $\mathbf{v}_{AB} = \begin{bmatrix} \mathbf{v}_A^T & \mathbf{v}_B^T \end{bmatrix}^T$ is introduced from the nodal velocities $\dot{\mathbf{H}}_A = \mathbf{H}_A\widetilde{\mathbf{v}}_A$ and $\dot{\mathbf{H}}_B = \mathbf{H}_B\widetilde{\mathbf{v}}_B$.

7. Discretized static formulation

7.1. Discretized static equilibrium equations

Starting from Eq. (37), the variation of the deformations in terms of the nodal values is needed for the computation of the internal forces of the finite element discretization.[1] It is straightforwardly obtained by combining Eqs. (64) and (65)

$$\delta(\boldsymbol{\epsilon}) = \delta\left(\frac{\mathbf{d}}{L}\right) = \frac{1}{L}\mathbf{P}(\mathbf{d})\delta\mathbf{h}_{AB} \tag{72}$$

Since the deformation is constant over the element so is its variation. Introducing this results into Eq. (37) leads to the expression of the nodal internal forces, namely the 12×1 vector $\mathbf{g}_{intAB}$ defined as $\delta(\mathcal{W}_{int}) = \delta\mathbf{h}_{AB}^T\mathbf{g}_{intAB}$

$$\mathbf{g}_{intAB}(\mathbf{d}) = \mathbf{P}(\mathbf{d})^T\mathbf{K}\boldsymbol{\epsilon} \tag{73}$$

The integration over the length of the element is trivial since all the terms are constant over the element. Moreover, the quantities involved in the evaluation of the nodal strain forces depend on the nodal values, $\mathbf{H}_A$ and $\mathbf{H}_B$, only through the relative configuration vector $\mathbf{d}$, meaning that they are invariant under rigid body motions and that they only vary according to the relative motion of the nodes.

The evaluation of the external forces requires the discretized expression of $\delta\mathbf{h}$ in Eq. (69). Inserting this into Eq. (40) yields the expression of the nodal external forces, namely the 12×1 vector $\mathbf{g}_{extAB}$ defined as $\delta(\mathcal{W}_{ext}) = \delta\mathbf{h}_{AB}^T\mathbf{g}_{extAB}$

[1] An equivalent expression of the discretized internal forces can be obtained starting from the weak form given in Eq. (41), but the choice made here simplifies the development.

$$\mathbf{g}_{extAB} = \int_0^L \mathbf{Q}(s,\mathbf{d})^T \mathbf{g}_{ext}\, ds \tag{74}$$

The external forces must be expressed in the material frame, so that forces that are naturally expressed in the inertial frame, e.g., the gravity forces, involve explicitly the position and orientation of the beam nodes.

Eventually, the finite element discretization yields a twelve-dimensional non-linear equilibrium equation for the unknown $\mathbf{H}_A$ and $\mathbf{H}_B$

$$\mathbf{g}_{intAB} - \mathbf{g}_{extAB} = \mathbf{P}(\mathbf{d})^T \mathbf{K}\boldsymbol{\epsilon} - \int_0^L \mathbf{Q}(s,\mathbf{d})^T \mathbf{g}_{ext}\, ds = \mathbf{0} \tag{75}$$

where we recall that $\mathbf{d}$ and $\boldsymbol{\epsilon}$ are computed from $\mathbf{H}_A$ and $\mathbf{H}_B$ using Eqs. (56) and (64). Applying boundary conditions (see the discussion in Section 7.2) would allow one to solve them for the relative configuration vector $\mathbf{d}$. Due to the Lie group framework, a Lie group static solver must be used to solve these equations. In this paper, a static version of the dynamic algorithm proposed in [8] and briefly recalled in Appendix B is used.

Due to the non-linearity of the static equilibrium equations in Eq. (75), an iterative process is necessary. This requires the evaluation of the tangent stiffness matrix. The contribution of the internal forces to the tangent stiffness matrix is obtained by considering the variation of Eq. (73), that is

$$\delta(\mathbf{P}(\mathbf{d})^T \mathbf{K}\boldsymbol{\epsilon}) = \mathbf{K}_T \delta\mathbf{h}_{AB} = \underbrace{\mathbf{P}(\mathbf{d})^T \mathbf{K} \frac{\mathbf{P}(\mathbf{d})}{L}}_{=\mathbf{K}_{Tm}} \delta\mathbf{h}_{AB} + \underbrace{\left(D\mathbf{P}(\mathbf{d})^T \cdot \delta\mathbf{h}_{AB}\right)\mathbf{K}\boldsymbol{\epsilon}}_{=\mathbf{K}_{Tg}\delta\mathbf{h}_{AB}} \tag{76}$$

The material part $\mathbf{K}_{Tm}$ is obtained straightforwardly from Eq. (72) since $\mathbf{P}(\mathbf{d})$ and $\mathbf{K}$ are anyway needed for the evaluation of the internal forces, which appears as a practical implementation advantage. The development of the geometric part $\mathbf{K}_{Tg}$, which is proportional to the elastic forces, is not given here for conciseness and since it is *a priori* not necessary in a small deformation context. The contribution of the internal forces to the tangent stiffness matrix can be obtained by exact integration over the element and it is expressed in compact form. Moreover, the quantities involved in its evaluation depend on the nodal values, $\mathbf{H}_A$ and $\mathbf{H}_B$, only through the relative configuration vector $\mathbf{d}$, meaning that it is invariant under rigid body motions and only depends on the relative motion of the nodes.

The external forces may also contribute to the tangent stiffness matrix and this contribution is not given here either because it is assumed to play a negligible role compare to $\mathbf{K}_{Tm}$ in case of small deformations. Their contribution, however, must be expressed in the material frame, so that it may involve explicitly the position and orientation of the beam element.

Accordingly, only the material part of the tangent stiffness matrix is considered in the following. This strategy saves computation costs, and it is shown that the solution process still reaches convergence efficiently.

7.2. Boundary conditions

Regarding the boundary conditions, [25] shows that the $SE(3)$ formalism is particularly convenient since the Lie algebra elements $\delta\mathbf{h}_A$ and $\delta\mathbf{h}_B$ are related to screw motions. Hence, two different kinds of non-free supports can be represented straightforwardly, which are a clamped end at node i, i.e. $\delta\mathbf{h}_i = \mathbf{0}$, and a simply supported end at node i, i.e. $\delta\mathbf{h}_{i\Omega} = \mathbf{0}$. Accordingly, the related equations are removed from the set to be solved and can provide the reaction forces afterwards. A similar method can be applied whenever a node is fixed to the ground through a lower-pair joint. However, other boundary conditions, such as a rolling bearing, do not fall into this category and it turns out that their representation in the present Lie group setting involves a non-linear relationship, which can be described using additional constraint equations, as presented in [28].

7.3. Absence of locking

The finite element formulation of shear deformable beams with linear interpolation and exact spatial integration exhibits a shear locking phenomenon [1]. It can be discussed by considering the shear in a cantilever beam subjected to a bending moment at its free end. Theoretically, the shear strain should vanish since pure bending does not involve any shear. Numerically, such an element subjected to pure bending undergoes shear deformations, the shear energy does not vanish and a too stiff behaviour is observed. The locking effect can be observed by varying the slenderness b/L, i.e., the thickness-length ratio of the element. When b/L decreases, the incorrect contributions, due to shear stiffness, become more important than the correct contributions, due to bending stiffness. Hence, the locking increases when the b/L decreases. The problem can be classically removed by a reduced integration method that filters high order bending contributions to shear.

In order to discuss the locking in pure bending for non-linear formulations, two different aspects should be considered: the correctness of the forces and the convergence of the iterative process. First, it should be verified that the finite element forces computed for the analytical position and rotation fields yield the forces expected from strength of materials. It is not the case for standard methods, and specific manipulations as reduced integration must be introduced. Then, once the forces are correct, the iterative process should be checked. Since non-linear formulations require iterative solvers, it should be verified that the formulation, and in particular the tangent stiffness matrix, is suitable for the convergence of such a procedure. As discussed in the previous paragraph, the insensitivity to slenderness is the critical point to be verified. These two aspects

are considered in the following of this section and the proposed element formulation appears to be inherently locking free. In particular, it yields the correct forces for the analytical position and rotation fields and a negligible sensitivity to slenderness of the iterative process based on the material part of the tangent stiffness matrix is shown in a pure bending numerical test. As in Section 6.2, a pure bending in the *xy*-plane is considered for conciseness, but the discussion of this section is valid for bending in any plane.

Let us first consider the forces. As pointed out in Section 6.2, the non-linear interpolation formula can geometrically represent the exact displacement field and rotation field in pure bending. The evaluation of the finite element forces in Eq. (73) requires the bending stiffness $\mathbf{C}_\Omega = \mathrm{diag}(GJ, EI_t, EI_u)$, the relative configuration vector $\mathbf{d}_U = [L\ 0\ 0]^T$ and $\mathbf{d}_\Omega = L[0\ 0\ k]^T$ with $k = M/(EI_u)$, and the deformations $\boldsymbol{\gamma} = [0\ 0\ 0]^T$ and $\boldsymbol{\kappa} = [0\ 0\ k]^T$. Since $\boldsymbol{\gamma}$ vanishes, the nodal strain forces in Eq. (73) are

$$\mathbf{g}_{intAB} = \begin{bmatrix} \mathbf{0}_{3\times1} \\ -\mathbf{T}_{SO(3)}^T(-\mathbf{d}_\Omega)\mathbf{C}_\Omega\boldsymbol{\kappa} \\ \mathbf{0}_{3\times1} \\ \mathbf{T}_{SO(3)}^T(\mathbf{d}_\Omega)\mathbf{C}_\Omega\boldsymbol{\kappa} \end{bmatrix} = \begin{bmatrix} \mathbf{0}_{3\times1} \\ -[0\ 0\ EI_u k]^T \\ \mathbf{0}_{3\times1} \\ [0\ 0\ EI_u k]^T \end{bmatrix} \tag{77}$$

where the explicit expression of $\mathbf{T}_{SO(3)}$ is given in Eq. (A.6). Noticing that $\widetilde{\mathbf{d}}_\Omega(\mathbf{C}_\Omega\boldsymbol{\kappa}) = \mathbf{0}, \mathbf{T}_{SO(3)}^T(-\mathbf{d}_\Omega)\mathbf{C}_\Omega\boldsymbol{\kappa} = \mathbf{T}_{SO(3)}^T(\mathbf{d}_\Omega)\mathbf{C}_\Omega\boldsymbol{\kappa} = \mathbf{C}_\Omega\boldsymbol{\kappa}$. Hence, Eq. (77) matches the exact solution from strength of materials. Furthermore, the result does not depend on the slenderness of the element. This development demonstrates that the forces of the proposed finite element are inherently locking free.

Let us now consider the convergence of the iterative process based on the material part of the tangent stiffness matrix only. The pure bending of a 1 m long cantilever beam with a square cross-section of side length b and tip end bending moment $M = kEb^4/12$ is computed numerically. The chosen numerical values for the test are a curvature $k = \pi/(2L)$ and a Young's modulus E of $210e3$ MPa. If the element was to lock due to non-physical axial or shear contributions, it would happen when diminishing b/L. In order to vary the slenderness b/L of the beam, the length is kept constant and the thickness b is varied from $1e-1$ to $1e-4$ m. A similar test could be done by keeping the value of b constant and varying L. The results of the numerical computations are given in Fig. 3 and compared to the analytical solution (see Eq. (61)). There is a sensitivity to slenderness in the element, but Fig. 3 shows that it does not impede numerical convergence. After the first iteration, the error is similar for all slendernesses, and after the fourth iteration, an error that is comparable to computer precision is reached whatever the slenderness. In between, iterating allows the reduction of the error but the smaller b/L, the smaller the reduction of the error. This limited sensitivity to slenderness during the iteration process assesses the locking free behaviour of the proposed formulation.

7.4. Test cases

A few test cases are shown in this section in order to illustrate the performance of the method. Only the material part, $\mathbf{K}_{Tm}$, of the tangent stiffness matrix in Eq. (76) is taken into account.

7.4.1. Convergence analysis of a cantilever beam subjected to a fixed load

We consider a cantilever beam subjected to a fixed load at its end. The load is a uniformly distributed force over one tenth of the beam starting from the free end and has a nominal value of $3e4$ N, to be integrated over the elements. The solution is computed for a varying number of elements in order to observe the spatial convergence rate of the element formulation. The

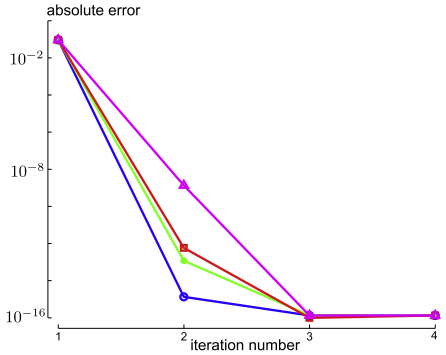

(a) Absolute error in horizontal displacement.

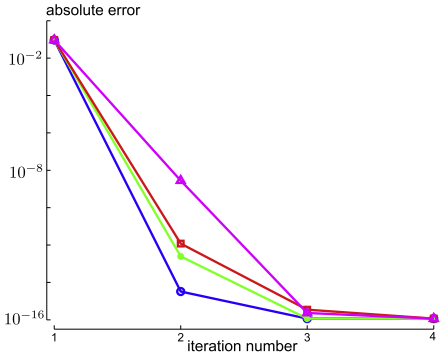

(b) Absolute error in vertical displacement.

Fig. 3. Cantilever beam subjected to a bending moment at the tip end. Absolute error in tip displacement at iteration numbers for different values of the slenderness: Circles (○): $1e-1$, Stars (★): $1e-2$, Squares (□): $1e-3$, Triangles (△): $1e-4$.

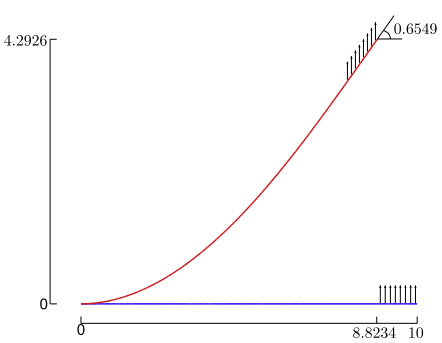

(a) Cantilever beam subjected to a uniformly distributed force at the tip end.

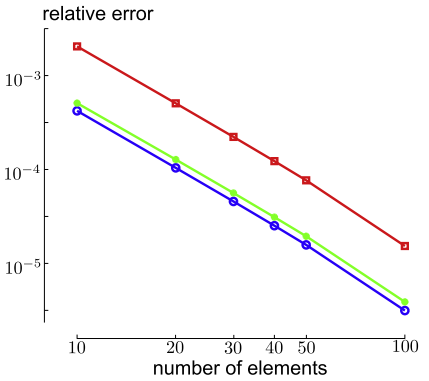

(b) Relative error.
Squares (□): Vertical displacement,
Stars (⋆): Rotation angle,
Circles (○): Horizontal displacement.

Fig. 4. Convergence analysis of a cantilever beam subjected to a fixed load.

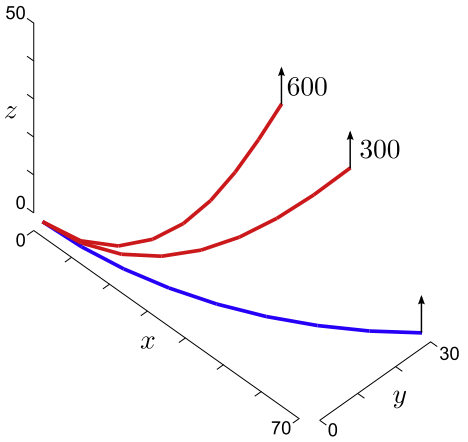

Fig. 5. Cantilever 45-degree bend subjected to a fixed load.

reference solution is computed with 200 elements. The numerical parameters of the case are: 10 m length, square cross-sections whose sides are 0.01 m long, Young's modulus $E = 210e3$ MPa and Poisson's ratio $\nu = 0.3$. The reference solution of the test case is presented in Fig. 4(a) and the relative errors are plotted in Fig. 4(b). A second-order spatial convergence is observed for the positions and rotations, which is consistent with the fact that the interpolation formula in Eq. (55) involves a linear polynomial interpolation in the Lie algebra.

7.4.2. Cantilever 45-degree bend subjected to a fixed load

We replicate the test case proposed in [29,30]. The bend lies initially in a plane, has a radius of curvature of 100 m and a unit square cross-section. The properties of the linear elastic material are the Young modulus $E = 10e7$ MPa and the Poisson ratio $\nu = 0$. The bend is discretized using 8 straight beam elements and the stopping criterion is a $1e-6$ relative error on the Euclidean norm of the residual. Two out-of-plane load cases are considered: 300 and 600 N. Each load is applied in one load step. The displacement results are plotted in Fig. 5 and are compared in Table 1 to those in [30]. The internal forces and moments are represented in Fig. 6. The convergence of the Newton iterative process is reached after 9 and 14 iterations for the 300 and the 600 N load case respectively.

7.4.3. Buckling of a hinged right-angle frame

We consider the planar problem of a right angle beam depicted in Fig. 7(a) (see e.g. [31]). The displacements at nodes A and B are fixed, but the in-plane rotations are allowed. A vertical force controlled by a load parameter λ, that is $F = \lambda * 1e3$, is exerted downwards at node D. Each side of the angle is discretized using 10 elements. This is a static buckling problem and

Table 1
Final tip position of a cantilever 45-degree bend subjected to an out-of-plane load.

	$SE(3)$ formulation			Simo and Vu-Quoc [30]		
Load	x	y	z	x	y	z
300	58.84	22.30	40.03	58.84	22.33	40.08
600	47.23	15.76	53.28	47.23	15.79	53.37

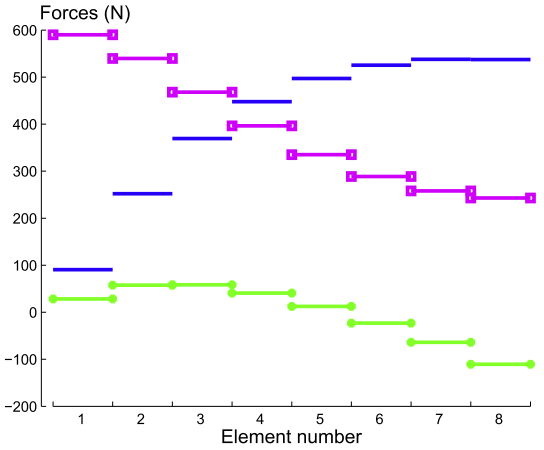

(a) Resulting forces. Line (–): axial force, Star (⋆): shear force t, Square (□): shear force u.

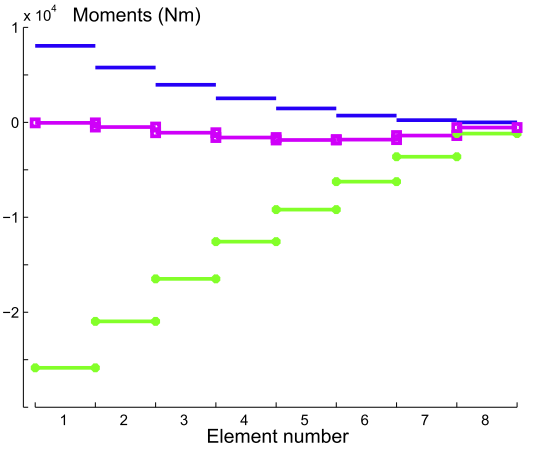

(b) Resulting moments. Line (–): torsion moment, Star (⋆): bending moment t, Square (□): bending moment u.

Fig. 6. Beam resultants Eqs. (32) and (33) expressed in the beam axes, that is $\mathbf{O}_0^T\mathbf{n}$ and $\mathbf{O}_0^T\mathbf{m}$, for the 600 N load case.

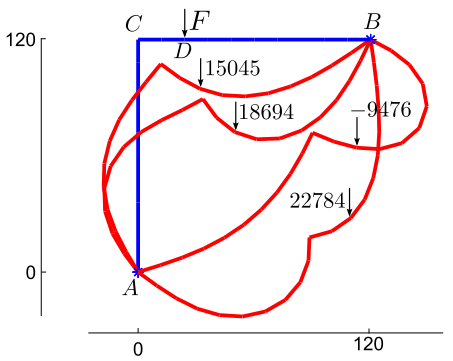

(a) A force controlled by parameter λ is exerted at node D. The displacements at node A and B are fixed, but rotations are free.

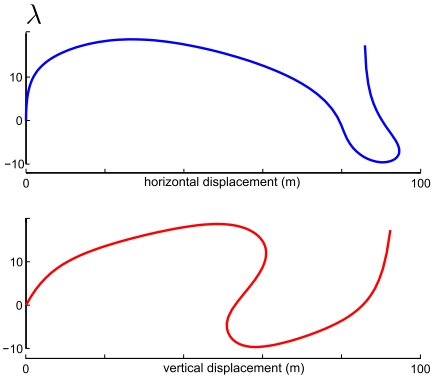

(b) Load parameter - Displacement of node C.

Fig. 7. Buckling of a two-dimensional hinged frame.

the continuation method in [32] has been adapted to the Lie group framework to solve the problem. The results obtained for the displacements of node C are showed in Fig. 7(b). They are in good agreement with [31].

7.5. Invariance of the tangent stiffness matrix: planar motion of a stiff beam attached to a wall

As mentioned earlier, the relative configuration vector $\mathbf{d}$ is invariant under rigid body motions and so is the tangent stiffness matrix $\mathbf{K}_T$. In order to reduce computational costs in the small deformation context, we suggest to keep the tangent stiffness matrix computed in the reference configuration for a whole simulation. The number of iterations might increase

since we neglect the deformation contributions, but the iteration matrix can be assembled and factorized only once for the whole simulation. In order to illustrate the advantage, let us consider a stiff initially horizontal beam hinged to a wall with a small rotational stiffness and subjected to a small vertical load at its free end. The beam is made of steel ($E = 210e3$ MPa and $\nu = 0.3$), 1 m long and has a square cross-section of area 0.01 m^2, the rotation stiffness at the wall is 100 N/radian and the vertical load at the free end is 50 N. The beam is discretized with 5 elements. The solution is plotted in Fig. 8. The beam undergoes large displacements but small relative motions of the nodes and the solution was obtained using the tangent stiffness matrix computed in the reference configuration.

In other application where the relative motions of the nodes within each element are not negligible, a non-systematic update procedure of the tangent stiffness matrix could be considered to optimize computational costs.

7.6. Summary

Thanks to the proposed Lie group framework, the deformations are naturally expressed in the material frame and the interpolation formula introduced in Section 6.1 implies that the deformations are approximated as being constant over a beam finite element. The nodal internal forces obtained from the virtual work principle can thus be integrated exactly and expressed in compact form. The material part of tangent stiffness matrix is obtained straightforwardly and a compact exact expression is available. The invariance under rigid body motions of the internal forces and of the tangent stiffness matrix stands out. In case of small relative motions of the nodes, the tangent stiffness matrix is almost constant even if the displacements are large, so that it is not necessary to update it for the iterative process to converge, provided that the relative motions remain small within each element. From an implementation point of view, it is worth noticing that the procedure is simple and that the computations at the element level only require the nodal orientations and positions.

8. Discretized dynamic formulation

8.1. Discretized dynamic equilibrium equations

From the dynamic equilibrium equations obtained using Hamilton's principle in Eq. (52), the following equation holds for the expression of the nodal inertia forces $\mathbf{g}_{ineAB}$

$$\delta\mathbf{h}_{AB}^T\mathbf{g}_{ineAB} = \int_0^L \delta\mathbf{h}^T(\mathbf{M}_C\dot{\mathbf{v}} - \widehat{\mathbf{v}}^T\mathbf{M}_C\mathbf{v})\, ds \tag{78}$$

Introducing the discretized expression of $\delta\mathbf{h}$ and $\mathbf{v}$ given in Section 6.3, the expression of the nodal inertia forces is given by

$$\mathbf{g}_{ineAB} = \int_0^L \left(\mathbf{Q}^T(\mathbf{M}_C\mathbf{Q}\dot{\mathbf{v}}_{AB} + \mathbf{M}_C\dot{\mathbf{Q}}\mathbf{v}_{AB} - \widehat{\mathbf{Q}\mathbf{v}_{AB}}^T\mathbf{M}_C\mathbf{Q}\mathbf{v}_{AB})\right) ds \tag{79}$$

where $\mathbf{Q} = \mathbf{Q}(s, \mathbf{d})$. This expression can be conveniently written in the following form

$$\mathbf{g}_{ineAB} = \mathbf{M}(\mathbf{d})\dot{\mathbf{v}}_{AB} + \mathbf{C}(\mathbf{d}, \mathbf{v}_{AB})\mathbf{v}_{AB} \tag{80}$$

where

$$\mathbf{M}(\mathbf{d}) = \int_0^L \mathbf{Q}^T\mathbf{M}_C\mathbf{Q}\, ds \tag{81}$$

$$\mathbf{C}(\mathbf{d}, \mathbf{v}_{AB}) = \int_0^L \mathbf{Q}^T(\mathbf{M}_C\dot{\mathbf{Q}} - \widehat{\mathbf{Q}\mathbf{v}_{AB}}^T\mathbf{M}_C\mathbf{Q})\, ds \tag{82}$$

Thanks to the interpolation method, the mass matrix $\mathbf{M}$ only depends on the relative configuration vector $\mathbf{d}$ and is thus exactly invariant under rigid body motions. The mass matrix is the exact tangent matrix for the linearization of the inertia

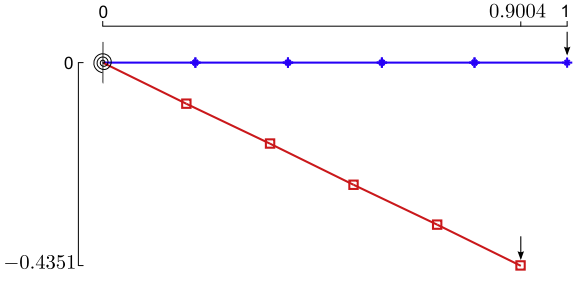

Fig. 8. Large displacement and small relative motions of the nodes of a stiff beam connected to a wall by a small rotational stiffness and subjected to a small vertical load at its free end.

forces with respect to the accelerations. $\mathbf{C}(\mathbf{d},\mathbf{v}_{AB})\mathbf{v}_{AB}$ are the gyroscopic forces. The exact time derivative of $\mathbf{Q}$ in $\mathbf{C}$ requires some developments which are given in C. Notice that the gyroscopic forces are quadratic in the velocity. Again, it is worth noticing that the inertia forces are naturally expressed in the material frame, so that the position and orientation of the beam nodes are involved only through the relative configuration vector $\mathbf{d}$.

Using the result from the static equilibrium in Eq. (75), the dynamic equilibrium equations take the form of ordinary differential equations on the Lie group

$$\dot{\mathbf{H}}_A = \mathbf{H}_A\widetilde{\mathbf{v}}_A \tag{83}$$

$$\dot{\mathbf{H}}_B = \mathbf{H}_B\widetilde{\mathbf{v}}_B \tag{84}$$

$$\mathbf{M}(\mathbf{d})\dot{\mathbf{v}}_{AB} + \mathbf{C}(\mathbf{d},\mathbf{v}_{AB})\mathbf{v}_{AB} + \mathbf{P}(\mathbf{d})^T\mathbf{K}\boldsymbol{\epsilon} = \int_0^L \mathbf{Q}(s,\mathbf{d})^T\mathbf{g}_{ext}\, ds \tag{85}$$

where $\mathbf{d} = \log_{SE(3)}(\mathbf{H}_A^{-1}\mathbf{H}_B)/L, \boldsymbol{\epsilon} = (\mathbf{d}-\mathbf{d}^0)/L$ and $\mathbf{v}_{AB} = \begin{bmatrix}\mathbf{v}_A^T & \mathbf{v}_B^T\end{bmatrix}^T$. These equations can be discretized in time and solved according, e.g., to the generalized-α Lie group time integrator presented in [8] and briefly recalled in B. The required numerical parameters are the time step size and the spectral radius.

8.2. Test cases

Two classical test cases are considered in order to assess the performance of the proposed discretized dynamic formulation. Following the discussion in Section 7.5 related to the invariance of the forces under rigid body motions, it is relevant to keep in Eq. (B.6) the tangent matrices of the reference configuration for the whole simulations as long as the relative motions in the elements remain small. This may increase the number of Newton iterations at each time step, but substantial gains in computational costs can be expected from the non-revaluation and non-refactorization of the iteration matrix. In the test cases of this section, the tangent damping matrix is neglected, and only the mass matrix and the material part of the tangent stiffness matrix are taken into account.

8.2.1. Free-free flexible beam with disks

We reproduce the test case described in [33]. A beam, as presented in Fig. 9, with rigid disks attached to it is subjected to an initial loading and the resulting free motion is observed. There are two out-of-plane loadings and one horizontal loading. These are applied according to $F(t)$, a function that increases linearly from 0 N to 20 N for $t \in [0, 2.5]$ s and decreases linearly from 20 N to 0 N for $t \in [2.5, 5]$ s. The disks have a mass of 10 kg and a rotation inertia $\mathbf{J} = \mathrm{diag}(200, 100, 100)$ kgm^2. The properties of the beam are $EA = GA = 1e4$ Nm^2, $EI = GI = 500$ Nm^4, the mass per unit length is 1 kg/m and the rotation inertia of the cross-sections is $\mathbf{J} = \mathrm{diag}(20, 10, 10)$ kgm. The simulation is run using 10 elements of equal length, a time step size $h = 0.1$ s and a spectral radius of 1. Disk B, as shown in Fig. 10(a), undergoes large amplitude motion in space and the energy is plotted in Fig. 10(b). The results are in good agreement with [33]. The relative motion of the beam nodes is small, so that the tangent matrix computed only once in the reference configuration can be used for the entire simulation. When the iteration matrix is updated, the mean number of iterations per time step is 4.44, while when the iteration matrix in the reference

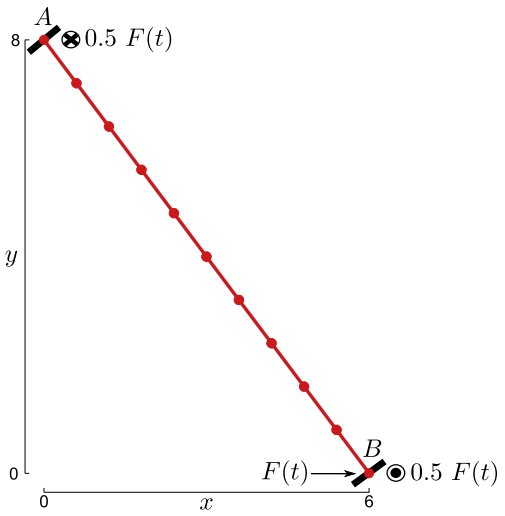

Fig. 9. Free-free beam with rigid disks attached to it at nodes A and B. Three forces are exerted: a horizontal force and an out-of-plane force at node B, and the opposite out-of-plane force at node A.

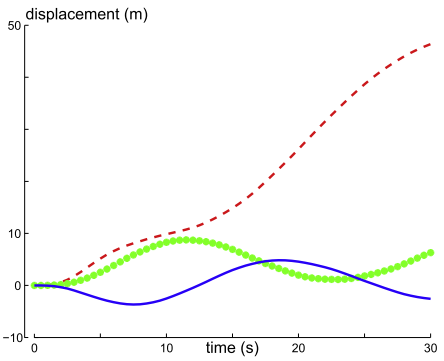

(a) Displacement of node B. Dashed line (- -): x, Doted line ($\star$): y, Solid line (–): z.

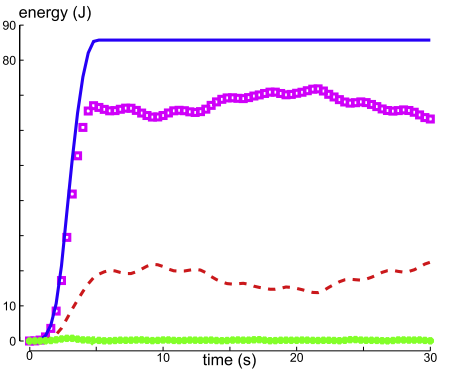

(b) Energy. Solid line (–): Total energy, Dashed line (- -): Kinetic energy of the beam, Doted line ($*$): Strain energy of the beam, Squares (□): Kinetic energy of the disks.

Fig. 10. Free-free flexible beam with disks.

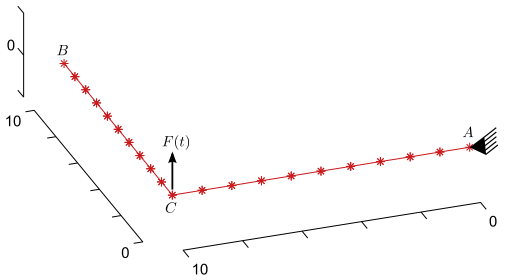

Fig. 11. Out-of-plane loading of a right angle beam: initial configuration. A force is exerted at node C during the first two seconds. Node A is clamped and node B is free.

configuration is kept, it is 5.03. Computational costs are thus significantly reduced since in the second case, the iteration matrix is computed and factorized only once.

8.2.2. Out-of-plane loading of a right angle beam

The right angle beam depicted in Fig. 11 is loaded by an out-of-plane concentrated force $F(t)$ at point C and the beam is clamped at node A. $F(t)$ increases linearly from 0 to 50 N for $t \in [0, 1]$ s, and then decreases linearly from 50 to 0 for $t \in [1, 2]$ s. The motion of the beam is observed during 30 s at nodes B and C. In particular, the motion after the loading is a large amplitude free vibration. Each side of the angle is 10 m long. The mechanical properties are $EA = GA = 1e6$ N, $EI = GJ = 1e3$ Nm^2, the mass per unit length is 1 kg/m and $\mathbf{J} = \mathrm{diag}(20, 10, 10)$ kgm. The out-of-place displacements and the energy are plotted in Fig. 12. They are in good agreement with those in [34]. For different spatial and time discretization, the mean number of Newton iterations is presented in Table 2. For every case, the spectral radius is $\rho = 0.9$. As it can be expected, the finer the space and time discretizations, the smaller the mean number of iteration per time step, but the higher the computation costs. Indeed, the predictions of the generalized-α scheme are better for a finer time discretization so that convergence is more easily achieved, but more time steps are computed. Regarding the spatial discretization, a higher number of elements reduces the relative motion of the nodes within each element, so that the non-linearities are reduced, but the higher number of variables increases the computation costs. However, it appears that with 10 elements per segment and a $1e-2$ s time step, the element relative motions are small enough to enable the problem to be solved using the iteration matrix computed in the reference configuration. An increase in the mean number of Newton iterations is observed since the iteration matrix is not the exact linearization of the equilibrium equations in the deformed configuration. Nevertheless, computation costs are saved since the iteration matrix is computed and factorized once, while in the other cases, it is computed and factorized at each iteration.

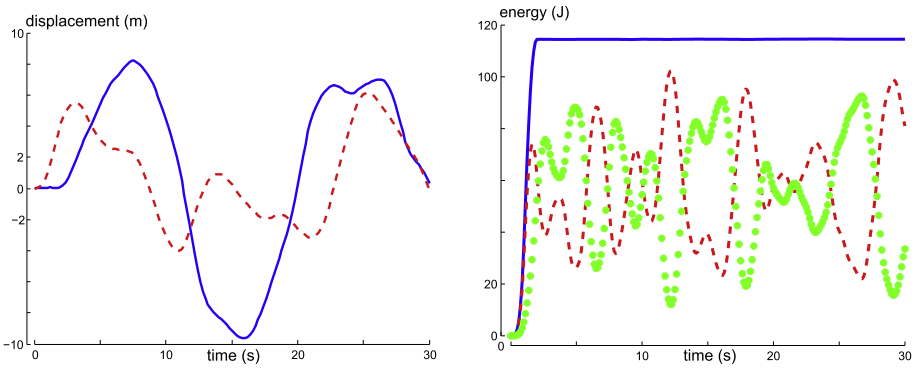

(a) Out-of-plane displacements. Solid line (–): Node B, Dashed line (- -): Node C.

(b) Energy. Solid line (–): Total energy, Dashed line (- -): Kinetic energy, Doted line (*): Strain energy.

Fig. 12. Results obtained with $h = 1e-1$ s and 10 elements for the out-of-plane loading of a right angle beam.

Table 2
Mean number of iterations per time step for different time and spatial discretizations of the right angle beam. Updated: the iteration matrix is updated at each time step, Frozen: the iteration matrix in the reference configuration is kept for the whole simulation.

	4 elements	10 elements
$h = 1e-1$ s	Updated: 3.6933 Frozen: no convergence	Updated: 3.2833 Frozen: no convergence
$h = 1e-2$ s	Updated: 1.9157 Frozen: no convergence	Updated: 1.3543 Frozen: 4.776

8.3. Summary

The interpolation of the velocities that is consistent with the configuration interpolation can be developed compactly using the $SE(3)$ formalism. The inertia forces are then straightforwardly obtained from Hamilton's principle. Since no parameterization of the global motion is introduced, they only depend on the nodal accelerations, the nodal velocities and the relative configuration vector. From an implementation point of view, it is worth noticing that the procedure is simple and that the computations at the element level only require the nodal values of the element at the current time step.

The test cases show that geometrically non-linear problems involving small relative motion in each element can be solved using a constant iteration matrix, computed from the mass matrix and the tangent stiffness matrix evaluated in the reference configuration.

9. Conclusions and perspectives

This paper addresses the formulation of a beam finite element in the Lie group framework, namely the special Euclidean group $SE(3)$.

Firstly, the static and dynamic equilibrium equations are developed in the $SE(3)$ framework. Their intrinsic nature is highlighted, namely the homogeneous equations do not depend on the configuration of the beam.

Based on this rigorous and systematic formalism, a non-linear interpolation formula using the exponential map is introduced. This method leads to a natural coupling of the position and rotation variables. The interpolation formula introduces a relative configuration vector which describes the relative motion of the nodes. Hence, the invariance property under rigid body motion comes naturally. Thanks to the interpolation formula, the deformation measures do not depend on the coordinate along the neutral axis of the beam and the internal forces, derived from a variational principle, can be integrated exactly over the element. It is shown that a locking free behaviour appears naturally due to the coupling of the position and rotation variables. The inertia forces are obtained from Hamilton's principle and rely on the consistent interpolation of the velocities with the spatial discretization.

The implementation procedure is simple. Indeed, the developments are conducted without introducing a global parameterization of the motion, and the forces are computed directly from the nodal values so that no intermediate value needs to be stored and the beam element handles systematically large motions.

Both the static and the dynamic formulations are successfully tested in standard test cases from the literature. The proposed formulation exhibits good accuracy, efficiency and convergence properties. Eventually, it is shown that geometrically non-linear problems with small relative motions in each element can be solved using for the whole simulation the iteration matrix computed in the reference configuration.

As a perspective, the natural coupling properties of the formulation could be significantly profitable in the case of initially curved elements. The extension of the method to plate and shell elements could also be considered. The proposed formulation can advantageously be used in the multibody framework since rigid bodies [9] and mechanisms [28] can also be modelled efficiently in a finite element approach using the $SE(3)$ formalism. The simplicity of the framework is also beneficial for sensitivity analysis and optimzation [35]. In order to reduce significantly computation costs of large systems, numerical investigations would be of interest to show how to exploit efficiently the invariance property of the tangent matrices under rigid body motions.

Acknowledgment

The first author would like to acknowledge the Belgian National Fund for Scientific Research for its financial support (FRIA fellowship).

Appendix A. Lie group formulas

This appendix provides formulas for the numerical computations of the Lie group operators introduced in the paper. Here are the series developments of

- the exponential map:

$$\exp(\widetilde{\mathbf{x}}) = \sum_{i=0}^{\infty} \frac{\widetilde{\mathbf{x}}^i}{i!} \tag{A.1}$$

- the tangent application and its inverse:

$$\mathbf{T}(\mathbf{x}) = \sum_{i=0}^{\infty} (-1)^i \frac{\widehat{\mathbf{x}}^i}{(i+1)!}; \quad \mathbf{T}^{-1}(\mathbf{x}) = \sum_{i=0}^{\infty} (-1)^i B_i \frac{\widehat{\mathbf{x}}^i}{i!} \tag{A.2}$$

in which B_i are the first Bernoulli numbers.

- the logarithmic map:

$$\log(q) = \sum_{i=1}^{\infty} (-1)^{i+1} \frac{(q-e)^i}{i} \tag{A.3}$$

A.1. The special orthogonal group, $SO(3)$

The adjoint representation acting on vectors $\boldsymbol{\Omega} \in \mathbb{R}^3$ is simply given by $\mathrm{Ad}_{\mathbf{R}}(\boldsymbol{\Omega}) = \mathbf{R}\boldsymbol{\Omega}$, where $\mathbf{R} \in SO(3)$. As proposed in [36], the following notations are used throughout the section

$$\alpha(\mathbf{b}) = \frac{\sin(\|\mathbf{b}\|)}{\|\mathbf{b}\|}; \beta(\mathbf{b}) = 2\frac{1-\cos(\|\mathbf{b}\|)}{\|\mathbf{b}\|^2}; \tag{A.4}$$

where $\mathbf{b} \in \mathbb{R}^3$. Notice that $\alpha(\mathbf{0}) = \beta(\mathbf{0}) = 1$. The exponential map has a compact analytical form given by Rodrigues' formula

$$\exp_{SO(3)}(\boldsymbol{\Omega}) = \mathbf{I}_{3\times 3} + \alpha(\boldsymbol{\Omega})\widetilde{\boldsymbol{\Omega}} + \frac{\beta(\boldsymbol{\Omega})}{2}\widetilde{\boldsymbol{\Omega}}^2 \tag{A.5}$$

Notice that $\exp_{SO(3)}$ is not injective. The tangent application is given by

$$\mathbf{T}_{SO(3)}(\boldsymbol{\Omega}) = \mathbf{I}_{3\times 3} - \frac{\beta(\boldsymbol{\Omega})}{2}\widetilde{\boldsymbol{\Omega}} + \frac{1-\alpha(\boldsymbol{\Omega})}{\|\boldsymbol{\Omega}\|^2}\widetilde{\boldsymbol{\Omega}}^2 \tag{A.6}$$

The inverse of the tangent application is given by

$$\mathbf{T}^{-1}_{SO(3)}(\boldsymbol{\Omega}) = \mathbf{I}_{3\times 3} + \frac{1}{2}\widetilde{\boldsymbol{\Omega}} + \frac{1}{\|\boldsymbol{\Omega}\|^2}\left(1 - \frac{\alpha}{\beta}\right)\widetilde{\boldsymbol{\Omega}}^2 \tag{A.7}$$

The logarithmic map is given by

$$\log_{SO(3)}(\mathbf{R}) = \widetilde{\boldsymbol{\omega}} = \frac{\theta}{2\sin(\theta)}(\mathbf{R} - \mathbf{R}^T) \tag{A.8}$$

with $\theta = \text{acos}\left(\frac{1}{2}(\text{trace}(\mathbf{R}) - 1)\right),\ |\theta| < \pi$. If $\mathbf{R} = \mathbf{I}_{3\times 3}, \theta = 0$ and $\widetilde{\boldsymbol{\omega}} = \mathbf{0}_{3\times 3}$.

A.2. The special Euclidean group, SE(3)

The adjoint representation acting on vectors of $\mathbb{R}^6$ is given by

$$\text{Ad}_{\mathbf{H}}(\mathbf{h}) = \begin{bmatrix} \mathbf{R} & \widetilde{\mathbf{x}}\mathbf{R} \\ \mathbf{0}_{3\times 3} & \mathbf{R} \end{bmatrix} \mathbf{h} \tag{A.9}$$

The exponential map is given by

$$\exp_{SE(3)}(\mathbf{h}) = \begin{bmatrix} \exp_{SO(3)}(\mathbf{h}_\Omega) & \mathbf{T}^T_{SO(3)}(\mathbf{h}_\Omega)\mathbf{h}_U \\ \mathbf{0}_{3\times 1} & 1 \end{bmatrix} \tag{A.10}$$

The tangent application is given by

$$\mathbf{T}_{SE(3)}(\mathbf{h}) = \begin{bmatrix} \mathbf{T}_{SO(3)}(\mathbf{h}_\Omega) & \mathbf{T}_{U\Omega+}(\mathbf{h}_U, \mathbf{h}_\Omega) \\ \mathbf{0}_{3\times 3} & \mathbf{T}_{SO(3)}(\mathbf{h}_\Omega) \end{bmatrix} \tag{A.11}$$

where

$$\mathbf{T}_{U\Omega+}(\mathbf{a}, \mathbf{b}) = \frac{-\beta}{2}\widetilde{\mathbf{a}} + \frac{1-\alpha}{\|\mathbf{b}\|^2}\lceil \mathbf{a}, \mathbf{b}\rceil + \frac{\mathbf{b}^T\mathbf{a}}{\|\mathbf{b}\|^2}\left((\beta - \alpha)\widetilde{\mathbf{b}} + \left(\frac{\beta}{2} - \frac{3(1-\alpha)}{\|\mathbf{b}\|^2}\right)\widetilde{\mathbf{b}}^2\right) \tag{A.12}$$

with $\alpha = \alpha(\mathbf{b}), \beta = \beta(\mathbf{b})$ and $\lceil \mathbf{a}, \mathbf{b}\rceil = \widetilde{\mathbf{a}}\widetilde{\mathbf{b}} + \widetilde{\mathbf{b}}\widetilde{\mathbf{a}}$. Notice that $\mathbf{T}_{U\Omega+}(\mathbf{a}, \mathbf{0}) = -\widetilde{\mathbf{a}}/2$. The inverse of the tangent application reads

$$\mathbf{T}^{-1}_{SE(3)}(\mathbf{h}) = \begin{bmatrix} \mathbf{T}^{-1}_{SO(3)}(\mathbf{h}_\Omega) & \mathbf{T}_{U\Omega-}(\mathbf{h}_U, \mathbf{h}_\Omega) \\ \mathbf{0}_{3\times 3} & \mathbf{T}^{-1}_{SO(3)}(\mathbf{h}_\Omega) \end{bmatrix} \tag{A.13}$$

where

$$\mathbf{T}_{U\Omega-}(\mathbf{a}, \mathbf{b}) = \frac{1}{2}\widetilde{\mathbf{a}} + \frac{\beta - \alpha}{\beta\|\mathbf{b}\|^2}\lceil \mathbf{a}, \mathbf{b}\rceil + \frac{1 + \alpha - 2\beta}{\beta\|\mathbf{b}\|^4}(\mathbf{b}^T\mathbf{a})\widetilde{\mathbf{b}}^2 \tag{A.14}$$

Notice that $\mathbf{T}_{U\Omega-}(\mathbf{a}, \mathbf{0}) = \widetilde{\mathbf{a}}/2$. The logarithmic map brings an element of the Lie group to the Lie algebra and is defined as

$$\log_{SE(3)}(\mathcal{H}(\mathbf{R}, \mathbf{x})) = \begin{bmatrix} \widetilde{\boldsymbol{\omega}} & \mathbf{T}^{-T}_{SO(3)}(\boldsymbol{\omega})\mathbf{x} \\ \mathbf{0}_{1\times 3} & 0 \end{bmatrix} \tag{A.15}$$

where $\widetilde{\boldsymbol{\omega}} = \log_{SO(3)}(\mathbf{R})$.

Appendix B. Lie group solver

The semi-discrete equations of motion can be solved using the Lie group version of the generalized-α scheme, as proposed in Ref. [8]. This algorithm preserves the Lie group structure of the problem. It has a proven second-order convergence and some numerical damping can be used to lessen the high frequency content. As in Section 2, q denotes the configuration state on the Lie group, $\mathbf{v}$ is the velocity and $\dot{\mathbf{v}}$ the acceleration. Denoting the inertia forces by $\mathbf{g}_{ine}$, the internal forces by $\mathbf{g}_{int}$ and the external forces by $\mathbf{g}_{ext}$, the integration method relies on the discretized equations involving the exponential map

$$q_{n+1} = q_n \exp(\widetilde{\mathbf{x}}_{n+1}) \tag{B.1}$$

$$\mathbf{g}_{ine}(\mathbf{v}_{n+1}, \dot{\mathbf{v}}_{n+1}) + \mathbf{g}_{int}(q_{n+1}) - \mathbf{g}_{ext} = \mathbf{0} \tag{B.2}$$

and the time integration formulae

$$\mathbf{x}_{n+1} = h\mathbf{v}_n + (0.5 - \beta)h^2\mathbf{a}_n + \beta h^2\mathbf{a}_{n+1} \tag{B.3}$$

$$\mathbf{v}_{n+1} = \mathbf{v}_n + (1 - \gamma)h\mathbf{a}_n + \gamma h\mathbf{a}_{n+1} \tag{B.4}$$

$$(1 - \alpha_m)\mathbf{a}_{n+1} + \alpha_m\mathbf{a}_n = (1 - \alpha_f)\dot{\mathbf{v}}_{n+1} + \alpha_f\dot{\mathbf{v}}_n \tag{B.5}$$

where n refers to the time step and h is the time step size. The numerical parameters of the integrator can be selected to achieve a desired spectral radius $\rho \in [0, 1)$ at high frequency:

$$\alpha_m = \frac{2\rho - 1}{\rho + 1}; \quad \alpha_f = \frac{\rho}{\rho + 1}; \quad \gamma = 0.5 + \alpha_f - \alpha_m; \quad \beta = \frac{(\gamma + 0.5)^2}{4}$$

At each time step, this set of equations is solved for the unknown $\mathbf{x}_{n+1}, \mathbf{v}_{n+1}, \dot{\mathbf{v}}_{n+1}$ and $\mathbf{a}_{n+1}$ by a Newton iterative procedure. The linearization of Eq. (B.1) gives $\Delta\mathbf{q}_{n+1} = \mathbf{T}(\mathbf{x}_{n+1})\Delta\mathbf{x}_{n+1}$ and the linearization of Eqs. B.3 and B.4 gives $\Delta\dot{\mathbf{v}}_{n+1} = (1-\alpha_m)/(\beta h^2(1-\alpha_f))\Delta\mathbf{x}_{n+1}$ and $\Delta\mathbf{v}_{n+1} = \gamma/(\beta h)\Delta\mathbf{x}_{n+1}$, where $\Delta(\bullet)$ denotes a small variation. Thus, the linearized form of Eq. (B.2) is

$$\Delta\mathbf{r} = \left(\frac{1-\alpha_m}{\beta h^2(1-\alpha_f)}\mathbf{M} + \frac{\gamma}{\beta h}\mathbf{C}_T + \mathbf{K}_T\mathbf{T}\right)\Delta\mathbf{x}_{n+1} \tag{B.6}$$

where Eq. (B.2) is denoted $\mathbf{r} = \mathbf{0}$ and $\mathbf{M}, \mathbf{C}_T$ and $\mathbf{K}_T$ are obtained by linearizing Eq. (B.2).

The solver can also be used in static cases, simply by removing the inertia forces from the equilibrium Eqs. (B.2) and removing the mass matrix $\mathbf{M}$ and the damping matrix $\mathbf{C}_T$ from the iteration matrix in Eq. (B.6). Index n refers then to the load step.

Appendix C. Computation of $\dot{\mathbf{Q}}$

The following computations rely on the concept of the directional derivative. Considering a function $f(\mathbf{x})$, the directional derivative in the direction $\mathbf{y}$ is defined as

$$Df(\mathbf{x}) \bullet \mathbf{y} = \lim_{t\to 0}\frac{f(\mathbf{x}+t\mathbf{y}) - f(\mathbf{x})}{t} \tag{C.1}$$

In particular, the time derivative is given by the directional derivative along the velocity vector, that is $\dot{f}(\mathbf{x},\dot{\mathbf{x}}) = Df(\mathbf{x}) \bullet \dot{\mathbf{x}}$, where $\dot{f}$ depends linearly on $\dot{\mathbf{x}}$.

Based on Eq. 70, the time derivative $\mathbf{Q}$ reads $\dot{\mathbf{Q}} = \begin{bmatrix} -\dot{\mathbf{T}}^* & \dot{\mathbf{T}}^* \end{bmatrix}$, where

$$\dot{\mathbf{T}}^*(s,\mathbf{h},\dot{\mathbf{h}}) = \frac{s}{L}\left(\dot{\mathbf{T}}\left(\frac{s}{L}\mathbf{h}\right)\ \mathbf{T}(\mathbf{h})^{-1} + \mathbf{T}\left(\frac{s}{L}\mathbf{h}\right)\left(\mathbf{T}(\mathbf{h})^{-1}\right)^{\cdot}\right) \tag{C.2}$$

and $\mathbf{T} = \mathbf{T}_{SE(3)}$. The explicit forms of $\dot{\mathbf{T}}$ and $(\mathbf{T}^{-1})^{\cdot}$ are given in the rest of the section. The compact notation relies on the two quantities $\alpha(\mathbf{b})$ and $\beta(\mathbf{b})$ defined in Eq. (A.4) as well as $\gamma(\mathbf{b}) = \alpha(\mathbf{b})/\beta(\mathbf{b}) = \frac{\|\mathbf{b}\|}{2}\cot\left(\frac{\|\mathbf{b}\|}{2}\right)$. The time derivative of these auxiliary quantities is given by

$$\dot{\alpha}(\boldsymbol{\Omega},\dot{\boldsymbol{\Omega}}) = \boldsymbol{\Omega}^T\dot{\boldsymbol{\Omega}}\left(\frac{(1-\alpha(\boldsymbol{\Omega}))}{\|\boldsymbol{\Omega}\|^2} - \frac{\beta(\boldsymbol{\Omega})}{2}\right) \tag{C.3}$$

$$\dot{\beta}(\boldsymbol{\Omega},\dot{\boldsymbol{\Omega}}) = \frac{2\boldsymbol{\Omega}^T\dot{\boldsymbol{\Omega}}}{\|\boldsymbol{\Omega}\|^2}(\alpha(\boldsymbol{\Omega}) - \beta(\boldsymbol{\Omega})) \tag{C.4}$$

$$\dot{\gamma}(\boldsymbol{\Omega},\dot{\boldsymbol{\Omega}}) = -\boldsymbol{\Omega}^T\dot{\boldsymbol{\Omega}}\left(\frac{1}{4} + \frac{\gamma(\boldsymbol{\Omega})(\gamma(\boldsymbol{\Omega})-1)}{\|\boldsymbol{\Omega}\|^2}\right) \tag{C.5}$$

In order to simplify the notations, the dependency on $\boldsymbol{\Omega}$ and on $\dot{\boldsymbol{\Omega}}$ of these definitions are not recalled and $\lceil\mathbf{a},\mathbf{b}\rceil = \tilde{\mathbf{a}}\tilde{\mathbf{b}} + \tilde{\mathbf{b}}\tilde{\mathbf{a}}$ is used.

Let us first compute the time derivative of the tangent application on $SO(3)$. We have

$$\dot{\mathbf{T}}_{SO(3)}(\boldsymbol{\Omega},\dot{\boldsymbol{\Omega}}) = \mathbf{T}_{U\Omega+}(\dot{\boldsymbol{\Omega}},\boldsymbol{\Omega}) \tag{C.6}$$

where $\mathbf{T}_{U\Omega+}$ was defined in Eq. (A.12). The time derivative $(\mathbf{T}_{U\Omega+}(\mathbf{a},\mathbf{b}))^{\cdot} = \dot{\mathbf{T}}_{U\Omega+}(\mathbf{a},\mathbf{b},\dot{\mathbf{a}},\dot{\mathbf{b}})$ is explicitly given by

$$\begin{aligned}
&-\frac{\beta}{2}\tilde{\dot{\mathbf{a}}} - \frac{\dot{\beta}}{2}\tilde{\mathbf{a}} + \frac{1-\alpha}{\|\mathbf{b}\|^2}\left(\lceil\dot{\mathbf{a}},\mathbf{b}\rceil + \lceil\mathbf{a},\dot{\mathbf{b}}\rceil\right) + \zeta(\mathbf{b}^T\dot{\mathbf{b}})\lceil\mathbf{a},\mathbf{b}\rceil \\
&+\frac{\alpha-\beta}{\|\mathbf{b}\|^2}\left((\dot{\mathbf{b}}^T\mathbf{a} + \mathbf{b}^T\dot{\mathbf{a}})\tilde{\mathbf{b}} + (\mathbf{b}^T\mathbf{a})\tilde{\dot{\mathbf{b}}}\right) + \zeta\left((\dot{\mathbf{b}}^T\mathbf{a} + \mathbf{b}^T\dot{\mathbf{a}})\tilde{\mathbf{b}}\tilde{\mathbf{b}} + (\mathbf{b}^T\mathbf{a})\lceil\dot{\mathbf{b}},\mathbf{b}\rceil\right) \\
&+\frac{(\mathbf{b}^T\dot{\mathbf{b}})\left(\mathbf{b}^T\mathbf{a}\right)}{\|\mathbf{b}\|^4}\left(\left(1 - 5\alpha - \frac{\beta}{2}\left(\|\mathbf{b}\|^2 - 8\right)\right)\mathbf{I}_{3\times 3} + \left(\alpha - \frac{7\beta}{2} + 15\frac{1-\alpha}{\|\mathbf{b}\|^2}\right)\tilde{\mathbf{b}}\right)\tilde{\mathbf{b}}
\end{aligned} \tag{C.7}$$

where $\alpha = \alpha(\mathbf{b}), \beta = \beta(\mathbf{b})$ and

$$\zeta = \zeta(\mathbf{b}) = \frac{1}{\|\mathbf{b}\|^2}\left(\frac{\beta}{2} - 3\frac{(1-\alpha)}{\|\mathbf{b}\|^2}\right) \tag{C.8}$$

Notice that when the second argument of $\dot{\mathbf{T}}_{U\Omega+}$ is zero, one has

$$\dot{\mathbf{T}}_{U\Omega+}(\mathbf{a},\mathbf{0},\dot{\mathbf{a}},\dot{\mathbf{b}}) = -\frac{1}{2}\tilde{\dot{\mathbf{a}}} + \frac{1}{6}\lceil\mathbf{a},\dot{\mathbf{b}}\rceil \tag{C.9}$$

Eqs. (C.6) and (C.7) lead straightforwardly to the time derivative of $\mathbf{T}_{SE(3)}$

$$\dot{\mathbf{T}}_{SE(3)}(\mathbf{x},\dot{\mathbf{x}}) = \begin{bmatrix} \dot{\mathbf{T}}_{SO(3)}(\mathbf{x}_\Omega,\dot{\mathbf{x}}_\Omega) & \dot{\mathbf{T}}_{U\Omega+}(\mathbf{x}_U,\mathbf{x}_\Omega,\dot{\mathbf{x}}_U,\dot{\mathbf{x}}_\Omega) \\ \mathbf{0}_{3\times3} & \dot{\mathbf{T}}_{SO(3)}(\mathbf{x}_\Omega,\dot{\mathbf{x}}_\Omega) \end{bmatrix} \tag{C.10}$$

In order to compute the time derivative of the inverse, that is $\mathbf{T}_{SE(3)}^{-1}$, the following derivatives are necessary

$$\left(\mathbf{T}_{SO(3)}^{-1}\right)^{\cdot}(\boldsymbol{\Omega},\dot{\boldsymbol{\Omega}}) = \frac{1}{2}\tilde{\dot{\boldsymbol{\Omega}}} + \frac{1}{\|\boldsymbol{\Omega}\|^2}\left((1-\gamma)\lceil\boldsymbol{\Omega},\dot{\boldsymbol{\Omega}}\rceil + \frac{\boldsymbol{\Omega}^T\dot{\boldsymbol{\Omega}}}{\|\boldsymbol{\Omega}\|^2}\left((\gamma-1)(\gamma+2)+\frac{\|\boldsymbol{\Omega}\|^2}{4}\right)\widetilde{\boldsymbol{\Omega}}\widetilde{\boldsymbol{\Omega}}\right) \tag{C.11}$$

$$\begin{aligned}\dot{\mathbf{T}}_{U\Omega-}(\mathbf{a},\mathbf{b},\dot{\mathbf{a}},\dot{\mathbf{b}}) = {}& \frac{1}{2}\tilde{\dot{\mathbf{a}}} + \frac{1-\gamma}{\|\mathbf{b}\|^2}\left(\lceil\dot{\mathbf{a}},\mathbf{b}\rceil + \lceil\mathbf{a},\dot{\mathbf{b}}\rceil\right) + \frac{\mathbf{b}^T\dot{\mathbf{b}}}{\|\mathbf{b}\|^4}\left((\gamma-1)(\gamma+2)+\frac{\|\mathbf{b}\|^2}{4}\right)\lceil\mathbf{a},\mathbf{b}\rceil \\ & + \frac{1/\beta+\gamma-2}{\|\mathbf{b}\|^4}\left((\dot{\mathbf{b}}^T\mathbf{a}+\mathbf{b}^T\dot{\mathbf{a}})\widetilde{\mathbf{b}}\widetilde{\mathbf{b}} + (\mathbf{b}^T\mathbf{a})\lceil\dot{\mathbf{b}},\mathbf{b}\rceil\right) \\ & + \frac{(\mathbf{b}^T\dot{\mathbf{b}})\left(\mathbf{b}^T\mathbf{a}\right)}{\|\mathbf{b}\|^6}\left(\frac{-2(\alpha+\beta)}{\beta^2} - \frac{\|\mathbf{b}\|^2}{4} - \gamma(\gamma+3)+8\right)\widetilde{\mathbf{b}}\widetilde{\mathbf{b}}\end{aligned} \tag{C.12}$$

where $\alpha = \alpha(\mathbf{b})$, $\beta = \beta(\mathbf{b})$ and $\gamma = \gamma(\mathbf{b})$. When the second argument of $\dot{\mathbf{T}}_{U\Omega-}$ is zero, one has

$$\dot{\mathbf{T}}_{U\Omega-}(\mathbf{a},\mathbf{0},\dot{\mathbf{a}},\dot{\mathbf{b}}) = \frac{1}{2}\tilde{\dot{\mathbf{a}}} + \frac{1}{12}\lceil\mathbf{a},\dot{\mathbf{b}}\rceil \tag{C.13}$$

Then, the time derivative of $\mathbf{T}_{SE(3)}^{-1}$ can be computed by

$$\left(\mathbf{T}_{SE(3)}^{-1}\right)^{\cdot}(\mathbf{x},\dot{\mathbf{x}}) = \begin{bmatrix} \left(\mathbf{T}_{SO(3)}^{-1}\right)^{\cdot}(\mathbf{x}_\Omega,\dot{\mathbf{x}}_\Omega) & \dot{\mathbf{T}}_{U\Omega-}(\mathbf{x}_U,\mathbf{x}_\Omega,\dot{\mathbf{x}}_U,\dot{\mathbf{x}}_\Omega) \\ \mathbf{0}_{3\times3} & \left(\mathbf{T}_{SO(3)}^{-1}\right)^{\cdot}(\mathbf{x}_\Omega,\dot{\mathbf{x}}_\Omega) \end{bmatrix} \tag{C.14}$$

References

[1] M. Géradin, A. Cardona, Flexible Multibody Dynamics: A Finite Element Approach, John Wiley & Sons, Chichester, 2001.
[2] O.A. Bauchau, Flexible mutibody dynamics, Solid Mechanics and its Applications, vol. 176, Springer, 2011.
[3] J. Simo, A finite strain beam formulation. The three-dimensional dynamic problem. Part I, Computer Methods in Applied Mechanics and Engineering 49 (1985) 55–70.
[4] J. Simo, D. Fox, On a stress resultant geometrically exact shell model. Part I: Formulation and optimal parametrization, Computer Methods in Applied Mechanics and Engineering 72 (1989) 267–304.
[5] A.A. Shabana, R.Y. Yakoub, Three dimensional absolute nodal coordinate formulation for beam elements: theory, Journal of Mechanical Design 123 (2001) 606–613.
[6] I. Romero, A comparison of finite elements for nonlinear beams: the absolute nodal coordinate and geometrically exact formulations, Multibody System Dynamics 20 (2008) 51–68.
[7] P. Betsch, P. Steinmann, Frame-indifferent beam finite elements based upon the geometrically exact beam theory, International Journal for Numerical Methods in Engineering 54 (2002) 1775–1788.
[8] O. Brüls, A. Cardona, M. Arnold, Lie group generalized-α time integration of constrained flexible multibody systems, Mechanism and Machine Theory (2012) 121–137.
[9] O. Brüls, M. Arnold, A. Cardona, Two Lie group formulations for dynamic multibody systems with large rotations, in: Proceedings of the IDETC/MSNDC Conference, Washington D.C., U.S.
[10] O. Brüls, A. Cardona, On the use of Lie group time integrators in multibody dynamics, ASME Journal of Computational and Nonlinear Dynamics 5 (2010) 031002.
[11] A. Cardona, M. Géradin, A beam finite element non-linear theory with finite rotations, International Journal for Numerical Methods in Engineering 26 (1988) 2403–2438.
[12] M. Crisfield, G. Jelenic, Objectivity of strain measures in the geometrically exact three-dimensional beam theory and its finite-element implementation, Proceedings of the Royal Society of London A 455 (1999) 1125–1147.
[13] M. Borri, C. Bottasso, An intrinsic beam model based on a helicoidal approximation – Part I: formulation, International Journal for Numerical Methods in Engineering 37 (1994) 2267–2289.
[14] P. Cesarek, M. Saje, D. Zupan, Dynamics of flexible beams: finite-element formulation based on interpolation of strain measures, Finite Elements in Analysis and Design 72 (2013) 47–63.
[15] J. McCarthy, An Introduction to Theoretical Kinematics, Cambridge, MIT Press, Mass, 1990.
[16] R.M. Murray, Z. Li, S.S. Sastry, A Mathematical Introduction to Robotic Manipulation, CRC Press, 1994.
[17] J. Angeles, Fundamentals of Robotic Mechanical Systems: Theory, Methods, and Algorithms, Springer-Verlag, Berlin, 2003.
[18] J.M. Selig, Geometric Fundamentals of Robotics, Monographs in computer science, Springer, New York, 2005.
[19] P. Crouch, R. Grossman, Numerical integration of ordinary differential equations on manifolds, Journal of Nonlinear Science 3 (1993) 1–33.
[20] H. Munthe-Kaas, Runge–Kutta methods on Lie groups, BIT 38 (1998) 92–111.
[21] C. Bottasso, M. Borri, Integrating finite rotations, Computer Methods in Applied Mechanics and Engineering 164 (1998) 307–331.
[22] F. Park, Distance metrics on the rigid-body motions with applications to mechanism design, Transactions of the ASME 117 (1995) 48–54.
[23] M. Zefran, V. Kumar, Interpolation schemes for rigid body motions, Computer-Aided Design 30 (1998) 179–189.
[24] O. Sander, Geodesic finite elements for Cosserat rods, International Journal for Numerical Methods in Engineering 82 (2010) 1645–1670.
[25] J.M. Selig, X. Ding, A screw theory of Timoshenko beams, Journal of Applied Mechanics 76 (2009) 031003.
[26] A. Iserles, H. Munthe-Kaas, S. Nrsett, A. Zanna, Lie-group methods, Acta Numerica 9 (2000) 215–365.
[27] W. Boothby, 2nd ed., An Introduction to Differentiable Manifolds and Riemannian Geometry, Academic Press, 2003.

[28] V. Sonneville, O. Brüls, Formulation of kinematic joints and rigidity constraints in multibody dynamics using a Lie group approach, in: Proceedings of the 2nd Joint International Conference on Multibody, System Dynamics (IMSD).
[29] K.-J. Bathe, S. Bolourchi, Large displacement analysis of three-dimensional beam structures, International Journal for Numerical Methods in Engineering 14 (1979) 961–986.
[30] J. Simo, L. Vu-Quoc, A three-dimensional finite-strain rod model. Part II: computational aspects, Computer Methods in Applied Mechanics and Engineering 58 (1986) 79–116.
[31] P. Jung, S. Leyendecker, J. Linn, M. Ortiz, A discrete mechanics approach to the Cosserat rod theory – Part 1: static equilibria, International Journal for Numerical Methods in Engineering 85 (2011) 31–60.
[32] A. Dhooge, W. Govaerts, Y.A. Kuznetsov, W. Mestrom, A.M. Riet, B. Sautois, MATCONT and CL MATCONT: continuation toolboxes in matlab, <www.matcont.ugent.be>, 2006.
[33] A. Ibrahimbegović, M.A. Mikad, Finite rotations in dynamics of beams and implicit time-stepping schemes, International Journal for Numerical Methods in Engineering 41 (1998) 781–814.
[34] E. Lens, A. Cardona, A nonlinear beam element formulation in the framework of an energy preserving time integration scheme for constrained multibody systems dynamics, Computers and Structures 86 (2008) 47–63.
[35] V. Sonneville, O. Brüls, Sensitivity analysis for multibody systems formulated on a Lie group, Multibody System Dynamics, 2013, in press.
[36] J. Park, W. Chung, Geometric integration on Euclidean group with application to articulated multibody systems, IEEE Transactions on Robotics 21 (2005) 850–863.